An episode of extremely high PM concentrations over Central Europe caused by dust emitted over the southern Ukraine

W. Birmili, K. Schepanski, A. Ansmann, G. Spindler, I. Tegen, B. Wehner, A. Nowak, E. Reimer, I. Mattis, K. Müller, et al.

**Atmospheric
Chemistry
and Physics
Discussions**

An episode of extremely high PM concentrations over Central Europe caused by dust emitted over the southern Ukraine

An episode of
extremely high PM
concentrations over
Central Europe

W. Birmili et al.

W. Birmili[1], K. Schepanski[1,2], A. Ansmann[1], G. Spindler[1], I. Tegen[1], B. Wehner[1],
A. Nowak[1], E. Reimer[3], I. Mattis[1], K. Müller[1], E. Brüggemann[1], T. Gnauk[1],
H. Herrmann[1], A. Wiedensohler[1], D. Althausen[1], A. Schladitz[1], T. Tuch[1,4], and
G. Löschau[5]

[1]Leibniz Institute for Tropospheric Research, Leipzig, Germany
[2]Leibniz Institute of Marine Sciences, IFM-GEOMAR, Kiel, Germany
[3]Institut für Meteorologie, Freie Universität Berlin, Germany
[4]Helmholtz Center for Environmental Research, Leipzig, Germany
[5]Sächsisches Landesamt für Umwelt und Geologie, Dresden, Germany

Correspondence to: W. Birmili (birmili@tropos.de)

Title Page	
Abstract	Introduction
Conclusions	References
Tables	Figures

◄◄	►►
◄	►
Back	Close

Full Screen / Esc

Printer-friendly Version

Interactive Discussion

EGU

Abstract

On 24 March 2007, the atmosphere over Central Europe was affected by an episode of exceptionally high mass concentrations of aerosol particles, most likely caused by a dust storm in the Southern Ukraine on the preceding day. At ground-based measurement stations in Slovakia, the Czech Republic, Poland and Germany PM_{10} mass concentrations rose to values between 200 and 1400 μg m^{-3}. An evaluation of PM_{10} measurements from 360 monitoring stations showed that the dust cloud advanced along a narrow corridor at speeds of up to 70 km h^{-1}. According to lidar observations over Leipzig, Germany, the high aerosol concentrations were confined to a homogeneous boundary layer of 1800 m height. The wavelength dependence of light extinction using both lidar and sun photometer measurements suggested the dominance of coarse particles during the main event. At a wavelength of 532 nm, relatively high volume extinction coefficients (300–400 Mm^{-1}) and a particle optical depth of 0.65 was observed. In-situ measurements with an aerodynamic particle sizer at Melpitz, Germany, confirmed the presence of a coarse particle mode with a mode diameter >2 μm, whose maximum concentration coincided with that of PM_{10}. A chemical particle analysis confirmed the dominance of non-volatile and insoluble matter in the coarse mode as well as high enrichments of Ti and Fe, which are characteristic of soil dust. A combination of back trajectory calculations and satellite images allowed to identify the dust source with confidence: On 23 March 2007, large amounts of dust were emitted from dried-out farmlands in the southern Ukraine, facilitated by wind gusts up to 100 km h^{-1}. The unusual vertical stability and confined height of this dust layer as well as the rapid transport under dry conditions led to the conservation of high aerosol mass concentrations along the transect and thus to the extraordinary high aerosol concentrations over Central Europe. Our observations demonstrate the capacity of a combined apparatus of in situ and remote sensing measurements to characterise such a dust with a variety of aerosol parameters. As a conclusion, the description of dust emission, transport and transformation processes needs to be improved, especially when facing the possible

effects of further anthropogenic desertification and climate change.

1 Introduction

1.1 Wind-blown dust and climate

Wind-blown dust particles emitted from dry soil surfaces contribute considerably to the
global aerosol mass and optical thickness, as well as to particle concentrations near
the surface. With the exception of sea salt particles, soil dust contributes globally the
highest atmospheric mass load of all aerosol particle types (Textor et al., 2006). Dust
particles are part of the coarse mode aerosol typically occurring in the super-μm size
range (Haywood et al., 2001; Reid et al., 2003). Current estimates of annual global
emission of dust particles that are available for long-range transport vary between 1000
and 2000 Tg (Zender et al., 2004). Frequent transport towards Europe of dust clouds
from the Sahara, the largest dust source worldwide, can be observed frequently within
the free troposphere (Ansmann et al., 2003; Barkan et al., 2005; Amiridis et al., 2005).
Atmospheric dust may therefore affect regional climates directly and indirectly by influ-
encing incoming and outgoing solar radiation, modifying cloud properties and precipita-
tion formation, and by affecting chemical processes in the atmosphere (Solomon et al.,
2007). The magnitudes of these effects depend on mineralogical, chemical and optical
particle properties as well as on the vertical extent of the dust clouds in the atmosphere
(Sokolik et al., 2001; Satheesh and Moorthy, 2005). A significant uncertainty factor in
quantifying dust fluxes is the lack of knowledge about emission potentials of different
source areas (Harrison et al., 2001).

Dust emissions are anticipated to change under changed climate conditions due
to alterations in both natural vegetation growth and cultivation patterns, as well as
changes in transport pathways (Mahowald and Luo, 2003; Tegen et al., 2004; Wood-
ward et al., 2005). Assessments of the role of dust in a different climates require the un-
derstanding of the controls on dust emission, including the role of changes in land use,

ACPD

7, 12231–12288, 2007

An episode of extremely high PM concentrations over Central Europe

W. Birmili et al.

Title Page

Abstract	Introduction
Conclusions	References
Tables	Figures

⏮   ⏭

◀   ▶

Back   Close

Full Screen / Esc

Printer-friendly Version

Interactive Discussion

EGU

as human activities can modify dust emissions from soils by changing the availability of fine particles, e.g., through destruction of soil crusts and removal of vegetation in semi-arid regions. The total amount of soil dust emission from such anthropogenic influence are currently estimated to contribute up to 20% of the total dust emissions (Solomon et al., 2007). However, such estimates are highly uncertain, as there are currently no appropriate measurements for quantifying large-scale dust emission fluxes.

1.2 Dust activation

Unvegetated areas containing fine and loose sediment can be sources of dust particle emission when strong surface winds occur. The Sahara is the most important source for soil dust worldwide; it is estimated to contribute at least 50% of the global atmospheric dust load (Goudie and Middleton, 2001). Ground dusts are mainly emitted via the process of saltation (Gillette, 1978; Shao et al., 1993; Marticorena and Bergametti, 1995), where sand particles that are easily lifted from the surface impact on the ground. There, the release of kinetic energy breaks the binding of finer soil particles like clay, which are then available for long-range transport. In some instances direct particle lifting has also been observed (Loosmore and Hunt, 2000), but this process is usually only of local importance. Strong winds are required to initiate and sustain dust emission from soils. These are often related to convective systems or the passages of cold fronts (Pye, 1987; Shao, 2000). Dust injected into high atmospheric levels of up to several kilometers can be transported over horizontal distances of thousands of kilometers by strong wind systems (Alpert et al., 2004).

Dust emissions are particularly strong in areas that contain fine and loose sediments. A good agreement has been found between the maximum occurrence of dust over land surfaces observed by satellites and the location of enclosed topographic depressions where fine sediment may have accumulated during the past (Prospero et al., 2002). The emission strength in a potential source region depends on surface properties like the aerodynamic surface roughness length, as structural elements like rocks or vegetation increase the transport of wind energy to the surface, but also partly absorb this

An episode of extremely high PM concentrations over Central Europe

W. Birmili et al.

Title Page

Abstract	Introduction
Conclusions	References
Tables	Figures

⏮   ⏭

◄   ►

Back   Close

Full Screen / Esc

Printer-friendly Version

Interactive Discussion

EGU

energy, increasing the threshold wind friction velocity required for dust emission (Marti-corena and Bergametti, 1995). The presence of crusts can reduce dust emission from a soil surface (Belnap and Gillette, 1997). The loss of fine soil material by wind defla-tion can lead to a decrease of dust production from a specific area over time (Gillette
5 and Chen, 2001). Surface disturbances as a consequence of cultivation of soils in dry regions may lead to enhanced dust emissions. In agricultural soils, particle mass fluxes depend on, among other parameters, soil wetness, plant growth, field size, and wind direction at field scales (Donk and Skidmore, 2003; Hagen, 2004).

1.3 Legal limit values for PM_{10}

10 Since 2005, legal limit values apply to environmental mass concentrations of PM_{10} within the European Community (Air Quality Framework Directive (96/62/EC) and First Air Quality Daughter Directive (1999/30/EC)). In practice, exceedances of the legal limit values, particularly the daily limit value of $50\,\mu g\,m^{-3}$ have occurred at air quality moni-toring stations in many EU member states frequently, and health scientists have called
15 for a more serious consideration of efficient abatement measures (Annesi-Maesano et al., 2007). The actual reasons for the PM_{10} exceedances are manifold, and may vary from region to region.

Several works have now examined the causes for the exceedances of the PM_{10} limit value in particular European regions: In the UK, which may be taken as representa-
20 tive for Western Europe, the advection of continental air masses as well as regional secondary aerosol formation seem to be responsible for the majority of exceedances of the daily limit value (Charron et al., 2007). In an arid region like Spain, in contrast, wind-blown dust, partially imported from the Sahara appear to play a major role (Es-cudero et al., 2007). In the metropolitan area of Berlin, Germany, 50% of the PM_{10}
25 mass concentration is estimated to originate from regional transport rather than local sources (Lenschow et al., 2001).

For Europe, not only desert dust transported from the Sahara desert may occasion-ally influence the atmospheric particle load but also dust particles blown off agricultural

An episode of extremely high PM concentrations over Central Europe

W. Birmili et al.

soils could contribute to particle concentrations. A synthesis of aerosol measurements from 24 stations in Europe (Putaud et al., 2004) finds that mineral aerosol is the main component in the $PM_{10-2.5}$ aerosol fraction, but is only of minor importance for the $PM_{2.5}$ fraction. In urban or rural areas dust from agricultural activities is sometimes assumed to be the cause for the PM_{10} mass balance deficit, since a considerable portion of the PM_{10} content in urban areas may originate from far-range transport. Underestimates of PM_{10} concentrations from air quality measurements have been suspected to be attributable to suspended agricultural soil dusts (Vautard et al., 2005).

Given the potential importance of soil dust aerosol for climate and air quality assessments and the possibility that dust emissions will change in future climates, improvements of our knowledge of dust sources and fluxes are essential.

In this paper we describe an exceptional dust event that greatly enhanced particle concentrations across Central Europe. The observations strongly suggest that most of this dust originated from a cultivated region within Europe. The body of observations provides the unique opportunity to characterize a case of anthropogenically induced soil dust emission and transport, which may ultimately help understanding of the changing role of soil dust aerosol under different climate conditions.

2 Measurement data and meteorological calculations

2.1 Satellite images

Due to the influence of dust particles infrared (IR) wavelength, airborne dust can be detected during daytimes and nighttimes by brightness temperature difference (BTD) (Ackerman, 1997; Wald et al., 1998; Sokolik, 2002; Brindley and Russell, 2006; Merchant et al., 2006). Different absorption and emission properties of dust and the Earth's surface at different thermal wavelength bands causes the BTD to decrease in the presence of airborne dust. To detect airborne dust by remote sensing, we use a dust index based on brightness temperature (BT) and BTD, converted from thermal IR radiances

measured by the SEVIRI (Spinning Enhanced Visible and InfraRed Imager) instrument on board the geostationary Meteosat Second Generation (MSG) satellite (Schmetz et al., 2002). The satellite is located at 3.5° W over the equator and has a horizontal resolution of 3 km at nadir and a time resolution of 15 min. The dust index is composed of the BTD at 12.0–10.8 μm and at 10.8–8.7 μm, as well as of the BT at 10.8 μm (Schepanski et al., 2007). It is based on the same BTs as EUMETSAT's dust index product of MSG scenes offered on its website (http://www.eumetsat.int, as of 11 June 2007).

In an alternative approach, mobilised dust can be identified in Moderate-resolution Imaging Spectroradiometer (MODIS) 721-composite pictures, using the near infrared (2155 nm) and two shortwave (876 nm, 670 nm) wavelength bands. The MODIS instrument flies on board of two polar-orbiting satellites, Terra and Aqua. True colour and composite pictures are available on the MODIS web site (http://rapidfire.sci.gsfc.nasa.gov/subsets, as of 11 June 2007) at 1 km, 500 m and 250 m horizontal resolution for predefined subsets. Here we use part of the Europe_2_04 Subset with a horizontal resolution of 250 m, imaged by the Earth Observing System (EOS) Aqua satellite on 23 March at 10:50 UTC. Due to its high reflectivity in the near infrared wavelength band (2155 nm) and its absorbent behaviour in the 670 nm and 876 nm wavelength bands, vegetation appears green in the composite picture. Bare soil causes a high reflectivity in all wavelength bands, especially in the 2155 nm wavelength band, so they can be identified by a brownish colour.

2.2 Lidar and Sun photometer observations

A low-cost, small and compact, semi-automated Raman lidar routinely monitors the troposphere over Leipzig (Althausen et al., 2004). For daytime periods, the vertical profile of the particle extinction coefficient at 532-nm wavelength is determined from the elastically backscattered aerosol signal. The extinction profile can be retrieved in a well-mixed boundary layer if a sun photometer observation of the total particle optical depth is available (Ansmann and Müller, 2005), as is the case here. Due to the

Title Page

Abstract | Introduction

Conclusions | References

Tables | Figures

|◄ | ►|

◄ | ►

Back | Close

Full Screen / Esc

Printer-friendly Version

Interactive Discussion

EGU

incomplete overlap of the laser beam with the receiver field of view, the retrieval of the profile is generally restricted to heights above about 400 m.

Leipzig is also an Aerosol Robotic Network (AERONET) site (Holben et al., 1998). The Leipzig sun photometer measures the particle optical depth at the 8 wavelengths, 340, 380, 440, 500, 675, 870, 1020, and 1640 nm continuously. AERONET data can be accessed through its corresponding website (http://aeronet.gsfc.nasa.gov, as of 11 June 2007).

2.3 PM$_{10}$ network observations

PM$_{10}$ mass concentrations are measured on a routine basis in every member state of the EU. For this paper we evaluated time series from more than 360 governmental air pollution monitoring stations in Slovakia, the Czech republic, Austria, Poland, and Germany. Most data were available at a time resolution of 30 min and generally measured by either the Tempered Oscillating Microbalance (TEOM) (Allen et al., 1997), or beta-gauge attenuation (Macias and Husar, 1976). A complete overview of the institutions that have supplied PM$_{10}$ data and the number of monitoring stations involved is given in Table 1 in Appendix A.

2.4 In situ measurements in Saxony

In-situ measurements of atmospheric aerosols were conducted during the dust episode at a number of measurement sites in Saxony, Germany. The most comprehensive set of measurements was carried out at the atmospheric research station Melpitz (51.2° N, 12.9° E), operated by the Leibniz Institute for Tropospheric Research near Leipzig. Atmospheric aerosols arriving in different air mass types at Melpitz have been widely characterised regarding their physical and chemical features (Neusüss et al., 2002; Spindler et al., 2004; Birmili et al., 2001; Engler et al., 2006), and Melpitz has also been a focal site for the comparison of aerosol characterisation techniques (Müller et al., 2004).

During the observation period between 23 and 25 March 2007, particle number size distributions in a size range between 3 and 800 nm were measured using a twin differential mobility particle sizer (TDMPS). This instrument is based on a parallel combination of two differential mobility analysers and determines electromobility size distributions (Birmili et al., 1999). In addition, coarse particle number size distributions were measured across the aerodynamic particle size range between 0.8 and 10 μm using an aerodynamic particle sizer (model 3321, TSI Inc., St Paul, USA; see Peters and Leith, 2003).

Both TDMPS and APS data were combined to obtain a complete particle number size distribution from 3 nm to 10 μm. This requires a transformation of the APS distributions from aerodynamic to electromobility diameter using an effective density of 2.0 g cm^{-3}, which complies with the average properties of mineral dust (e.g., Maring et al., 2003). Also, TDMPS and APS size distributions were corrected for particle losses in the ambient aerosol inlet. Here, we accounted for transport losses of small particles due to Brownian diffusion in laminar flow, as well as sedimentation losses along horizontal sections of the inlet pipe, which were calculated using analytical formulae (Hinds, 1999; Brockmann, 2001).

Since particles larger than the upper size limit of the TDMPS instrument (800 nm) were not removed physically, the multiple charge inversion of the mobility raw distributions requires the knowledge of the concentrations of larger particles. As the size distribution of coarse particles was obtained by APS measurements, their effect could be accounted for prior to the TDMPS charge inversion. The calculation, presented in more details in Appendix B, showed that the contribution of coarse particles to the sub-μm raw mobility distribution was not negligible during the dust event and about 40% at maximum.

Particle number size distributions were also recorded at two governmental air pollution monitoring sites in Saxony, Niesky (51.3° N, 14.8° E) and Schwartenberg (50.7° N, 13.5° E). Here, a TDMPS with a particle size range of 3–800 nm, and a scanning mobility particle sizer (SMPS) with a size range of 10–800 nm were deployed, respectively.

An episode of extremely high PM concentrations over Central Europe

W. Birmili et al.

The SMPS was based on a single differential mobility particle sizer in conjunction with a condensation particle counter (model 3010, TSI Inc.).

Size fractionated particle mass concentrations of PM_{10}, $PM_{2.5}$ and PM_1 were measured at Melpitz using a GRIMM Environmental Dust Monitor (EDM, model 107, Grimm Inc., Ainring, Germany). This instrument uses a semiconductor laser as light source to monitor the light scattering of single particles. Ambient aerosol was sampled at a flow rate of $1.2 \, l \, min^{-1}$. The device generates a clean and particle-free sheath air stream which passes through the optical chamber and serves to prevent dust contamination in the laser-optic system and as a zero reference air during the auto-calibration procedure. As single particles pass through the laser beam in the optical chamber, light scattering occurs and is culminated by a mirror that is located 90° from the laser source and measured by a recipient diode. The signal of that diode is recorded by a multi-channel size classifier. A pulse height analyzer then classifies the transmitted signal in each channel. Conversions from the measured particle number to volume and from volume to mass distribution are performed using internal protocols developed by Grimm Inc. For Melpitz, we found that the PM mass concentrations measured by EDM have been very similar to those measured by the reference methods (TEOM and filters sampling).

The EDM deployed at Melpitz is additionally equipped with a specially designed heated inlet in order to realize measurements at different inlet temperature. The air temperatures in these two separate inlet lines correspond to ambient temperatures (10°C at maximum on 24 March 2007), and 50°C, respectively. The sampling line leading to the EDM is switched between ambient temperature and 50°C every half hour so that both measurements can be compared. A temperature of 50°C is, in particular, sufficient to evaporate nitrate compounds prior to analysis (see, e.g., Hildemann et al., 1984). The interested reader may also be referred to the work by Grover et al. (2006), who discuss recent comparison experiments of the EDM with alternative volatility characterisation techniques.

An episode of extremely high PM concentrations over Central Europe

W. Birmili et al.

Title Page

Abstract	Introduction
Conclusions	References
Tables	Figures

◄ | ►◄

◄ | ►

Back | Close

Full Screen / Esc

Printer-friendly Version

Interactive Discussion

2.5 Particle sampling and chemical analysis

At the Saxonian observation sites Melpitz, Niesky, Schwartenberg, as well as Dresden-Nord and Dresden-Herzogingarten (both 51.0° N, 13.7° E) aerosol particles were collected using PM_{10} and $PM_{2.5}$ high volume filter samplers (DHA-80, Digitel Elektronik,
Hegnau, Switzerland). The samples were collected over 24 h on 150 mm quartz fibre filters (MK 360, Munktell Filter AG, Falun, Sweden). After equilibration at 50% relative humidity the filters were weighed and divided for the subsequent analyses as described in Plewka et al. (2004).

The analysis of ionic components followed standard methods of ion chromatography (Metrohm) and capillary electrophoresis (Spectrophoresis1000). For a detailed description of these methods we refer to Brüggemann and Rolle (1998) and Neusüss et al. (1999). Organic and elemental carbon (OC/EC) were analysed by a two-step thermographic method using a non-dispersive infrared (NDIR) carbon analyser (C-mat 5500, Ströhlein, Düsseldorf, Germany). The method, extensively described in Plewka et al. (2004) is a variation of the official guideline VDI 2465 (Part 2, 1999). Metal analyses were carried out by inductively coupled plasma optical emission spectrometry (ICP-OES) according to DIN EN ISO 11885.

2.6 Back trajectory calculations

3d-backward trajectories were calculated to determine transport patterns and source regions for the dust particles observed over Central Europe. For the period between 15 March and 1 April 2007 backward trajectories were determined by fine mesh analysis (Reimer and Scherer, 1992). The back trajectories were started at 20 receptor locations in Germany using 10 minute time steps. The trajectory technique utilises an isentropic coordinate system as well as a mixed dynamical/kinematical scheme with a sigma surface at the lower boundary. The column contacts of all trajectories on 24 March 2007 were integrated for a 1 km^2 grid over Europe. For each site three types of trajectories were started: A first one driven by the 3d-wind field only, a second one with

a relative vertical velocity of 0.5 mm s^{-1} and third one with a relative vertical velocity of 1.0 mm s^{-1}. The vertical velocities were introduced to account for the gravitational settling and correspond to dust particle diameters of 2.8 and 4.0 μm, respectively. For each trajectory the parameters pressure, height and date were collected at the grid cells and the resulting local mean values for each grid were determined by considering the local contact frequency.

3 Meteorological overview

3.1 Synoptic overview

On 20 March 2007, four days prior to the dust observations, the synoptic situation of Europe was governed by a low pressure area over Northern to Southern Europe (see Fig. 1, top chart), built-up by eastward travelling depressions located over Scandinavia and the west Mediterranean region. Both depressions correspond to an extensive vertical cold-air pool. In front of the Mediterranean low pressure system North African air masses with dust were transported to the North. From 21 to 24 a permanent anticyclone was located over East Europe and Fennoscandinavia with dry continental air travelling to central Europe, as depicted in the bottom chart of Fig. 1. The depression over the West Mediterranean, which had stayed relatively immobile until 24 March, started to move eastwards. The combination of the eastward-moving depression, the anticyclone over South Russian and the cold-air pool to the high pressure region over East and North Europe forced a strong easterly wind over the Black Sea and the southern Ukraine on 23, 24 March, continuing until 25 March. The high wind speeds over the southern Ukraine and the transport corridor featuring high wind speeds are displayed in Fig. 2. Importantly, the distribution of the pressure systems effected a transport of a dry and subsiding air mass form the Black Sea area to Central Europe along a narrow corridor: Starting in the morning on 23 March over the Southern Ukraine, the air mass was transported across the Ukraine, Slovakia, Poland, the Czech Republic, and

An episode of extremely high PM concentrations over Central Europe

W. Birmili et al.

reached Germany on 24 March. The transect was characterised by high wind speeds of more than $50\,km\,h^{-1}$ and a low humidity north of the frontal line indicated in the bottom chart of Fig. 1.

3.2 Back trajectories

₅ The exact pathway of the air mass arriving in Central Europe was verified through backward trajectory computations. Bundles of back trajectories arriving at 20 receptor sites in Germany are shown in Fig. 3. The calculations were made for particles without gravitational settling, and for particles with sedimentation velocities of 0.5 and $1.0\,mm\,s^{-1}$, which corresponds to dust particle diameters of 2.8 and $4.0\,\mu m$, respectively.

₁₀ In analogy to the wind field shown in Fig. 2 the trajectory model predicts a strongly channelled flow from the region of the Caspian Sea over Ukraine towards Central Europe (see Fig. 3 (centre graph) with red and magenta areas). Air from the northern shore of the Black Sea is predicted to reach Germany within only 18 to 24 h. The low-level dust cloud is pictured by yellow and green colours in Fig. 3 (bottom graph),
₁₅ showing that between the Ukraine and the receptor area, all trajectories moved at heights below 1500–1600 m. The trajectory calculations cover the movement of the dry air mass depicted in Fig. 1, and reproduce the spatial distribution of the PM_{10} peak values, which is shown later.

It is noticeable that the back trajectory calculations allow the transport of particles
₂₀ into Central Europe in air from southerly directions, which merge with the easterly flow over the southern Ukraine. Such a transport across the Mediterranean is, however, only possible if gravitational settling of particles is taken into account. All air masses considered subsided on 22 and 23 March over south-eastern Europe and formed the low level jet towards Central Europe

3.3 Satellite images

Due to its high spatio-temporal resolution dust source activation and dust transport can be tracked with the SEVIRI instrument at high accuracy (Sect. 2.1). Fig. 4 shows SEVIRI's MSG dust index image on 23 March, 11:00 UTC, which reveals a strong event of dust emission over the Southern Ukraine, as indicated by magenta colour. Due to continuing high wind speeds, even a second event of dust source activation could be detected on the following day, 24 March. The dust emission shown in Fig. 4 is located exactly on the pathway that leads the air mass from this region to Central Europe.

A more detailed view of the source region can be seen in Fig. 5, which shows the southern and eastern area of the Kahkova Reservoir. The MODIS Aqua composite picture confirms the dust emission, which occurs over an area of approximately $20\,000\,km^2$. Brown stripes of dust can be seen over the blue-black colour of the reservoir, indicating dust mobilised from agricultural soil. In fact, the composite picture is not very sensitive for airborne dust, and the colour of the dust can be seen to agree with the colour of the surface, which consists of agricultural soil. Southern Ukraine is known for its fertile black earth (Chernozem), which has been intensively used for agriculture in the past and can, to date, be classified as erodible soil.

Interestingly, the dust emission and transport can be seen to take place along lengthy filaments, located between 1.5 and 3 km apart (Fig. 5). On 23 March, local meteorological observations over the southern and eastern area around the Kahkova Reservoir report average wind speeds up to $50\,km\,h^{-1}$ and wind gusts up to $90\,km\,h^{-1}$, and also confirmed the "observation of atmospheric dust". Radiosounding observations in Kiev (23 March, 12:00 UTC) show a logarithmic wind speed profile that reached a maximum of 50 Kn at an altitude of 1500 m. It is likely that these unusually high surface wind speeds in combination with a preceding drought period of two weeks as well as the low roughness length due to lack of vegetation in March led to the high dust emission rates.

It is noteworthy that in MSG dust index images (not shown) the dust cloud could be

detected from about 24 March, 00:00 UTC over Germany again, albeit in a reduced fashion after 08:00 UTC due to a cover of non-precipitating clouds.

While it may be theoretically possible that the dust cloud arriving at Central Europe contained significant contributions of Saharan dust, two arguments diminish the likeli-
hood of this option: First, Saharan dust can only enter into Central Europe in significant amounts via lofted aerosol layers (Ansmann et al., 2003; Barkan et al., 2005; Amiridis et al., 2005). If being transported through the planetary boundary layer, precipitation on the northern shores of the Mediterranean would usually quickly remove dust aerosol particles. In lofted aerosol layers dust concentrations remain relatively stable, but would
need to mix with boundary layer air in order to be detectable on the ground, as was the case on 24 March. Due to the necessary vertical dilution process, a multiple of the near-ground mass concentration would have been needed in such a lofted layer of Saharan dust.

A second argument is that Saharan dust would have been required to pass over
Turkey and the Black Sea in order to merge over the southern Ukraine with the easterly flow from from the Caspian Sea (Fig. 3). On 23 March, there were numerous cloudless satellite scans over Turkey and the Black Sea, but in fact, no quantities of dust could be detected there in the satellite images. Therefore, we conclude that the dust cloud observed on 24 March in Central Europe originates overwhelmingly from the source
identified in the southern Ukraine.

4 Aerosol measurements in Central Europe

4.1 Observations within the PM_{10} network

4.1.1 Time series of PM_{10}

Exceptionally high concentrations of airborne particulates were observed on 24 March
2007 at numerous governmental air pollution monitoring stations in Slovakia, the Czech

republic, Poland, Austria and Germany. Figure 6 illustrates the time series of PM_{10} at a number of selected monitoring stations. As can be seen in the figure, the concentrations were below $50\,\mu g\,m^{-3}$ at most stations – occasionally around $100\,\mu g\,m^{-3}$, before the arrival of the dust layer. The first station to detect the dust event was Košice in Eastern Slovakia (48.7° N, 21.2° E) in the late evening of 23 March, when the concentrations augmented dramatically within a matter of two hours (Fig. 6).

During the entire day of 24 March, the dust cloud was transported in westerly direction, thereby traversing Central Europe in a confined band. PM_{10} concentrations increased up to $1400\,\mu g\,m^{-3}$ in Slovakia in the morning of 24 March, and up to $600\,\mu g\,m^{-3}$ in Germany during mid-day. Importantly, the event could be seen as a clear, outstanding peak in the time histories of all monitoring stations crossed by the dust cloud, regardless whether the station was a rural or urban background station, or even a roadside station.

4.1.2 Geographic mapping of the dust event

Figure 7 shows the map of peak PM_{10} mass concentrations during the dust event, generated from observational data at a total number of about 360 monitoring stations (cf. Table 1). The PM_{10} time series at all monitoring stations traversed by the dust cloud showed a pronounced maximum, and were similar in shape to those shown in Fig. 6. In order to simplify the amount of data, all individual time series were parametrised by Gaussian model curves, thereby yielding two parameters: (a), the peak value of PM_{10} concentration and, (b) the time of occurrence of this maximum.

The advancement of the dust cloud across Central Europe is visualised in Fig. 7. Shown are the frontal lines that indicate the temporal evolution of the dust cloud as well as the peak PM_{10} concentrations occurring along the pathway. Remarkably, the highest PM_{10} concentrations occurred in Slovakia and the Małopolskie voivodeship in Poland, which are the areas the closest to the source region in Ukraine. The other most affected areas include the Czech Republic and the State of Saxony in Germany. It can be seen that the dust cloud moved faster across the south of Poland than across

An episode of extremely high PM concentrations over Central Europe

W. Birmili et al.

the Czech Republic. Two reasons are responsible for this, the flatter terrain in Poland and the decrease of the wind speed towards the south, where the centre of the low pressure system resides.

After passing across Northern Germany, the dust cloud eventually reached the North Sea in the afternoon of 24 March. In fact, the traces of the dust could still be detected over Southern England, as indicated from UK Automatic Particulate Monitoring Network data (not shown here). A time lag analysis of the multiple station data across Central Europe suggests that the air mass was moving at relatively constant speeds around $70\,km\,h^{-1}$.

It is noteworthy that towards its southern edge, the dust cloud can be delimited with high accuracy because of the relatively dense coverage of Austria and Germany with PM_{10} network data. Meteorological observations reported a band of rainfall to the southern edge of the dust cloud, which is most likely one of the reasons why the dust particles did not penetrate further south. The eastern and northern edge of the dust cloud could not be defined with the same accuracy because of the unavailability of PM_{10} observation data, notably for the Ukraine and some voivodeships of Poland.

4.1.3 Estimation of the total amount of dust

The available spatial coverage of PM_{10} mass concentrations was used to full capacity when estimating the total mass of dust present in the atmosphere as a result of the dust storm. Since such an estimate will be the most accurate when examining the measurements close to source, we analysed the time series of PM_{10} data from stations that lay in the vicinity of the 04:00 CET frontal line that is shown in Fig. 7. Within the proximity of this frontal line lie, from north to south, the monitoring stations Tarnów and Nowy Sacz (both Poland), and Prešov, Krompachy, Košice, and Velká Ida (Slovakia).

First, the transversal dimension of the dust cloud was derived from Fig. 7. To determine the longitudinal dimension of the dust cloud, the flow field was split into separate volume elements passing across each of the 6 stations mentioned above from east to west. The speed of the air mass was determined for each volume element by deriving

the time lag of PM_{10} observations between different stations along the longitudinal axis. Thus, the time series of PM_{10} as a function of time could be transformed into curves of PM_{10} as a function of longitudinal dimension.

Finally, the vertical dimension of the of the dust cloud was estimated from vertical profiles of the virtual potential temperature recorded by radiosoundings in at Kiev, Poprad-Ganovce, Wrocław and Prague, resulting in an average of 1400 m across the entire area. It was assumed that the particles were evenly distributed within the boundary layer on the vertical axis, which is supported by the lidar profile observed further downwind (cf. Sect. 4.3). An integration over the entire concentration field then yielded an approximation for the total dust mass in the atmosphere.

Our calculation yielded a total dust mass of 60 Gg for the dust cloud at 04:00 CET. As a matter of PM_{10} sampling, the figure of 60 Gg can only include aerosol particles <10 μm in aerodynamic diameter. The mass of the total suspended dust may accordingly have been higher.

4.2 In situ measurements in Saxony

Particle number size distributions across a wide range (3 nm–10 μm) were recorded at the research station Melpitz using a twin differential mobility partcle sizer (TDMPS) and an aerodynamic particle sizer (APS). Figure 8 shows the particle number and volume size distributions derived from these number distributions as well as integral particle mass concentrations.

Figure 8 (top graph) reveals the presence of a coarse particle mode resulting from the advection of the air mass from Southern Ukraine on 24 March 2007. Although experiencing a concentration rise as early 00:00 CET, the coarse mode attained its maximum concentration in Melpitz at around 11:00 CET, and between 09:30 and 14:00 CET across Saxony. Clearly, this coarse particle mode represents an aerosol population that changes with time independently from the fine particle mode, and is separated from the fine mode by a concentration minimum at 1 μm. During its time of maximum concentration the coarse mode was characterised by a count median diameter around 2 μm

and a volume median diameter of about $3\,\mu$m. In the afternoon, the coarse mode concentrations gradually decreased towards their morning level. One day later (25 March, 14:00 CET) a second, albeit less pronounced episode of coarse dust can be seen.

A view at the size-fractionated mass concentrations (Fig. 8, lower top graph) confirms that the mass concentration of PM_{10} is almost entirely dominated by the coarser fraction. PM_1, which represents the fine mode, remains very constant throughout the entire day of 24 March, and $PM_{2.5}$ shows a diurnal variation by a factor of two. This implies that during the peak in coarse mode concentration, PM_{10} is made up to almost 75% by the size fraction $PM_{10-2.5}$

Simultaneous particle number size distribution measurements at three continental background observation sites across Saxony (Fig. 8, bottom graph) suggested that besides its relative constancy in time, the accumulation particle mode – marked by count mean diameters around 100 nm was rather homogeneously distributed in the horizontal dimension across at a few hundred kilometres. For PM_{10}, the data indicates a similar covariation across 14 measurement sites in Saxony (Fig. 8, centre graph).

It is of a certain interest that the occurrence of the second dust event on 25 March, 14:00 CET was associated with high concentrations of particles <40 nm as well as temporarily reduced concentrations of the accumulation mode. A decrease in the accumulation mode in the middle of the day can be indicative of vertical mixing with air from aloft. The observation therefore suggests that the coarse mode particles could be mixed down from a remotely transported layer aloft. The formation of the new particles <40 nm at all sites could likewise be associated to this mixing process, as this process tends to bring about favourable conditions for the formation of new particles (Nilsson et al., 2000, 2001).

Meteorological and gas phase chemical observations at the governmental air pollution stations (not shown here) yielded a covariations across Saxony regarding temperature, relative humidity, ozone and nitrogen dioxide concentrations, which is a further indicator for a spatially homogeneous air mass on 24 March. The relative humidity was very close to 100% during the evening of 23 March, but started to drop at midnight at all

An episode of extremely high PM concentrations over Central Europe

W. Birmili et al.

Title Page

Abstract	Introduction
Conclusions	References
Tables	Figures

⏮   ⏭

◀   ▶

Back   Close

Full Screen / Esc

Printer-friendly Version

Interactive Discussion

EGU

stations, beginning with the easternmost station Niesky in Saxony. During 24 March, the relative humidities decreased to values between 40 and 50% at the monitoring stations lower than 150 m above sea level, which confirms satellite observations (not shown) that the air advected from Southern Ukraine was very dry in relation both, to the preceding air mass as well as to the air mass in the centre of the low pressure system. The low relative humidities between 40 and 50% during 24 March also rule out any significant enhancement of aerosol optical depth by hygroscopic growth. Consequently, the optical observations described in the next section refer to an overwhelmingly dry aerosol.

The ground level wind speeds ranged between 2 and 12 m s^{-1} in Saxony, which is considerably lower than the 70 m s^{-1} resulting from the multiple site analysis.

4.3 Lidar and sun photometer observations

Figure 9 shows lidar observations that were recorded during the time of maximum dust concentration at Leipzig ("L" in Fig. 7). The vertical profile of the volume extinction coefficient suggests that the aerosol plume arriving on 24 March in Central Europe was confined to the lowest two kilometers of the troposphere. On 24 March, no lofted aerosol layers could be detected in the free troposphere, neither in the morning nor the early afternoon. Apparently, the aerosol layer originating from the northern shore of the Black Sea became well mixed during the long-range transport with strong winds. The lidar observations revealed a high particle optical depth of 0.65 and high extinction coefficients of 300 to 400 M m^{-1} at 532 nm throughout the dust layer in the early afternoon of 24 March 2007. The typical values of the particle optical depth at Leipzig are much lower, around 0.1 and 80–90 M m^{-1}, respectively (Mattis et al., 2004).

The fact that the dust plume could not penetrate into the free troposphere is considered to be the main reason for the high aerosol concentrations measured at ground. In fact, no lofting or mixing with clean free tropospheric air was possible during the transport. The height of the aerosol layer is highly consistent with radiosounding observations further upwind in Wrocław (Poland; 24 March, 00:00 UTC) and Lindenberg

An episode of extremely high PM concentrations over Central Europe

W. Birmili et al.

Title Page

Abstract	Introduction
Conclusions	References
Tables	Figures

◀ | ▶|

◀ | ▶

Back | Close

Full Screen / Esc

Printer-friendly Version

Interactive Discussion

(Germany; 24 March, 00:00, 06:00, and 12:00 UTC), which suggested mixed layer heights of 1700 m and 1500 m, respectively. A certain variation in the heights of the aerosol layer as well as the mixed layer as observed during the transect of the dust cloud is anticipated due to inhomogeneities in terrain as well as the synoptic evolution of the air mass. The radiosounding observations suggest a spatial variation in the mixed layer height of a few 100 m.

The AERONET sun photometer measured a particle optical depth of 0.64 at 500 nm at 13:02 UTC at the station IFT-Leipzig (see Fig. 10). The Ångström exponent of 0.55 derived for the wavelength interval 440–870 nm indicates the presence of a considerable fraction of coarse mode particles with diameters >1.2 μm. Meanwhile, the extinction-to-backscatter ratio (lidar ratio) of 60 sr retrieved from the combined AERONET (optical depth) and lidar observations (column-integrated backscatter co-efficient) show a clear signature of non-spherical soil or dust particles. In the case of a large fraction of large particles as measured at ground, the lidar ratio would be 20–25 sr according to Mie scattering theory, which assumes spherical particles. As shown during our previous long-term measurements, the lidar ratio for obviously non-spherical particles can be larger by a factor of 2–3 compared to spherical particles (Mattis et al., 2002).

The sun photometer measurements from 24 March 2007 in Fig. 10 are comple-mented by two cases featuring Sahara dust aerosol, one directly measured close to the Sahara, at Ouarzazate, Southern Marocco, on 15 May 2006, and another after a major transport event of Saharan dust to Leipzig on 14 October 2001 (Müller et al., 2003; Ansmann et al., 2003). The comparison of the Saharan dust and the Ukrainian soil dust spectra reveal that the aerosol on 24 March was composed of fine mode parti-cles (continental haze), indicated by a strong spectral dependence of the optical depth from 340–600 nm, and coarse mode particles which cause a similarly flat spectral slope of the optical depth in the range from 800–1700 nm as the Saharan dust particles. The contribution of anthropogenic fine mode particles to the total particle-related optical depth is estimated to be about 0.1. Thus 80% of the optical depth results from light

extinction by the soil dust.

4.4 Physico-chemical and chemical properties

4.4.1 Volatility of bulk PM at 50°C

Figure 11 shows the half-hourly time series of PM concentrations measured by the
Grimm Environmental Dust Monitor (EDM), which switches in an alternating fash-
ion between two inlets tempered at ambient temperatures and 50°C, respectively
(cf. Sect. 2.4). During the passage through the heated inlet air stream volatile com-
pounds, such as nitrate (Hildemann et al., 1984) are evaporated and deposited onto
the walls of the system.

PM_1 at Melpitz consists of relevant fractions of both, volatile and non-volatile material
(Fig. 11). The average fraction of material volatile at 50°C in PM_1 ranged between 11
and 67% on the three days shown and was on average 33%. In contrast, the coarse
particle fractions, $PM_{2.5-1}$ and $PM_{10-2.5}$ contained much less material volatile at 50°C,
only 14% and 3%, respectively.

Remarkably, the dust-associated mass concentration peak on March 24 (10:00–
14:00 CET) was related overwhelmingly to $PM_{2.5-1}$ and $PM_{10-2.5}$ and within these,
only 6% and 1% of the material could be accounted for by the volatile fraction. This
result adds up to the impression that the dust-related mass concentration peak is de-
lineated from the fine particle mode (PM_1), and made up mostly from crustal material.

For the data shown in Fig. 11 the mean mass concentrations for PM_{10} and $PM_{2.5}$
were 50.7 and 32.0 $\mu g\,m^{-3}$, respectively. It is noteworthy that these results are
in fair agreement with the corresponding bulk DIGITEL measurements of 49.1 and
32.8 $\mu g\,m^{-3}$. These results suggest that the Grimm EDM provides correct mass con-
centrations for the aerosol occurring at Melpitz.

EGU

4.4.2 Main components of bulk PM

Figure 12 gives an overview of the mass concentrations of selected compounds for daily samples of PM_{10} and $PM_{2.5}$ at Melpitz on 23, 24 and 25 March. Concentrations for $PM_{10-2.5}$ were calculated by subtracting the value of $PM_{2.5}$ from that of PM_{10}. On 23 March, PM_{10} and $PM_{10-2.5}$ were significantly increased by the impact of the dust cloud. PM_{10} reached a daily average value of $84\,\mu g\,m^{-3}$ on 24 March, the day of the dust cloud. The major mass gain from 23 to March 24 March is caused by the coarse fraction $PM_{10-2.5}$, which increased by a factor of 10.

The chemical speciation identified major amounts of soluble ions (ca. 30%) in $PM_{2.5}$ on March 23 and a total carbon (TC) fraction of about 8%. $PM_{10-2.5}$, in contrast, features only negligible amounts of soluble ions, but about 30% carbonaceous material, and an overwhelming fraction (∼70%) of unidentified material. The unidentified material contains those compounds that are neither soluble, ionic, nor carbonaceous. The major class representing this unidentified fraction in atmospheric aerosols is crustal material, which typically includes silicates and insoluble carbonates (e.g., Fernandez-Espinosa et al., 2002).

The air mass change from 23 March to 24 March featured, above all, an increase in the unidentified chemical fraction. This change is most notably in $PM_{10-2.5}$, where the unidentified fraction attains a share of ∼85%. This measurement is a further indicator for the presence of crustal material in the dust aerosol advected into Central Europe. On 25 March, the bulk PM composition changes again, now with a reduced share of unidentified material but an increased fraction of carbonaceous material, notably elemental carbon (Fig. 12). This can be taken as indicative of combustion processes taking place upwind the observation sites, and is not surprising based on this air mass' residence time of more than 6 days over land, as suggested by trajectory calculations.

4.4.3 Spatial variation of chemical composition

Since chemical analyses of bulk PM samples could be performed for various measurement sites in Saxony, we were able to examine the spatial homogeneity of the dust-influenced aerosol within a scale of a few 100 km. Figure 13 illustrates the bulk
5   chemical composition of PM_{10} at the five sampling stations Dresden-Nord (roadside), Dresden-Herzogingarten (urban background), Schwartenberg (rural), Niesky (rural) and Melpitz (rural). Besides for 24 March, data are shown for 28 March, comparison day featuring continental air originating in Eastern Europe as well. It is apparent from Fig. 13 that the spatial variation of chemical composition between the sites tends
10   to be much smaller than, for instance, the day-to-day variations between the different air masses sampled (see Figs. 12 and 13). In fact, no systematic deviation in chemical can be discerned at the urban background and roadside station for the dominating effect of dust material on PM_{10}.

4.4.4 Ti and Fe in in bulk PM_{10}

15   The time series of Fe and Ti concentration in daily samples is shown in Fig. 14. PM_{10} sampling was conducted on every fourth day within the framework of an aerosol characterisation experiment under the auspices of the Saxonian regional office for the environment and geology. Therefore, this data is not available for each day. Fortunately, one of the sampling days (24 March 2007) coincided with the day when the dust cloud
20   could be detected over Central Europe.

Figure 14 reveals that like PM_{10} mass concentrations, the concentrations of Fe and Ti show a pronounced peak on the day of the dust event. The highest concentrations of Fe and Ti were observed at the station Schwartenberg, $4.4\,\mu g\,m^{-3}$ and $0.36\,\mu g\,m^{-3}$, respectively. Schwartenberg is a mid-level mountain station 752 m a.s.l. close to the
25   Czech-German border (cf. Fig. 7), and it is probably a consequence of this location that the concentrations of these geogenic tracers is the highest here.

To assess the geogenic contributions to a particular particle sample, it can be useful

to compare the relative mass fraction of a substance in a PM sample to its relative abundance in the upper continental crust. Based on the data shown in Fig. 14, the mass fractions of Fe and Ti in PM_{10} were, as an average at the rural stations Schwartenberg, Niesky, and Melpitz, 3.2% and 0.24% respectively on 24 March. During the subsequent sampling event on 28 March the values were merely 1.1% (Fe) and 0.08% (Ti). These values give evidence that the high Fe and Ti concentrations on 24 March (Fig. 14) are not a result of the variation of total mass, but of the change in chemical composition along with the dust event.

Taylor and McLennan (1985) report crustal abundances of 3.50% (Fe) and 0.30% (Ti), which are of rather similar value as the 3.2% and 0.24% observed on 24 March 2007. It is known that Ti is an element that originates mainly from geogenic sources. A simple mass balance model assuming geogenic dust to be the only source of Ti leads to the result that 80% of the PM_{10} mass concentration observed on March 24 would be geogenic dust.

It is very interesting that the unidentified chemical species presented in Sect. 4.4.2 make up a mass fraction of 80% as well. An alternative figure is the non-volatile mass in the coarse particle size range 1–10 μm. This fraction, which can also be associated with crustal dust particles made up 68% on 24 March. The divergence from 80% can eventually be explained by the presence of some dust material in PM_1.

Unlike for Ti, a mass-balance assessment could not be carried out for Fe because there are significant anthropogenic sources, such as metal abrasion or tyre wear that contribute to ambient Fe concentrations. For urban aerosols in Birmingham, UK, Birmili et al. (2006) showed that the enrichment of Fe in environmental coarse PM (>1 μm) was one order of magnitude higher than in fine PM (<1 μm). Consequently, the coarse mode contributions are expected to control total Fe concentrations in urban PM. The observations of Fig. 14 agree with this effect as far as the Fe concentrations at the urban stations Dresden-Nord and Dresden-Herzogingarten were higher compared to the rural levels between 4 and 24 March. Here, the excess Fe can be attributed to the various urban sources in Dresden. On 24 March, the urban sources do not play

a crucial role due to the ruling effect of the remotely transported dust particles from southern Ukraine. Fe concentrations at Dresden-Nord and Dresden-Herzogingarten are between the values for the background stations Niesky and Schwartenberg.

In conclusion, several independent approaches come to the result that the mass fraction of dust in the daily average PM_{10} sample on 24 March was about 80%.

5 Discussion

5.1 Conditions for dust emission and transport

The reasons for the extreme values of PM_{10} in Central Europe were severalfold. On top of an aged continental air mass moving constantly from South-Easterly direction, coarse dust was activated in Southern Ukraine at extremely high wind speeds. This dust was transported within 24 h into Central Europe along a narrow pathway on the northern edge of a low pressure system. The unusual stability and limited height of this dust layer as well as the rapid transport under dry conditions (day-time relative humidity between 40 and 50%) was responsible for the unusually high mass concentrations of PM in Central Europe. Although an impact of Saharan dust cannot be ruled out based on the backtrajectory analysis (Sect. 3.2), the body of satellite and ground-based remote sensing observations make a significant contribution of Saharan dust unlikely.

5.2 Dust mass observed on 24 March 2007

On the basis of PM_{10} in Central Europe, an attempt was made to estimate the total mass of the dust cloud observed on 24 March 2007. The calculation was made for the frontal line of the dust cloud on 24 March, 04:00 CET, when large concentrations occurred over the Eastern parts of Slovakia and Poland (cf. Fig. 7). The calculation made use of the time series of PM_{10} at six measurement stations in Slovakia and Poland. The estimate of the total dust mass that passed the 04:00 UTC frontal line

during 8 hours was 60 Gg. This estimate is based on the upper cut-off of the PM_{10} sampling systems, and hence excludes particles larger than $10\,\mu m$.

5.3 How frequent does such dust transport occur?

The meteorological analysis in Sect. 3.2 as well as the profile measurements in Sect. 4.3 reveal the major reasons for the observation of the Ukrainian dust cloud in Central Europe: Extraordinary wind speeds in the source region after a two-week drought period, and very rapid transport of the activated dust to the receptor region within an unusually stable and confined boundary layer. The combination of these factors also raises the question how frequent such events may be expected over climatologically relevant durations.

To address this question, the existing long-term time series of daily PM_{10} mass concentrations and chemical composition between 1993 and 2007 at Melpitz was screened for similar dust events. As indicators for signficant dust events we employed (a) high PM_{10} mass concentrations $>100\,\mu g\,m^{-3}$, (b) a high mass fraction of chemically unidentified material (cf. 4.4.2, and (c) a corresponding low mass fraction of ionic compounds such as nitrate and sulphate.

It can be stated that over the years 1993–2007, no single day could be identified that had chemical composition features similar to the dust cloud observed on 24 March 2007. Therefore, the observed low-level dust cloud over Central Europe is assumed to occur only rarely, probably not more often than once in 10 years. Only two days were found whose parameters came close to its characteristics, December 28, 1996 (PM_{10} $116\,\mu g\,m^{-3}$, mass fraction of ionic compounds 27%) and December 11, 2002 (PM_{10} $104\,\mu g\,m^{-3}$, mass fraction of ionic compounds 27%). A back trajectory analysis showed that both air masses originated in Central Russia, but were not particularly related to high wind speeds, so that their unidentified chemical fraction cannot be attributed to a specific area such as on 24 March 2007.

An episode of extremely high PM concentrations over Central Europe

W. Birmili et al.

Title Page

Abstract	Introduction
Conclusions	References
Tables	Figures

|◄ | ►|

◄ | ►

Back | Close

Full Screen / Esc

Printer-friendly Version

Interactive Discussion

5.4 Source region Southern Ukraine

Although some influence by Saharan dust cannot be ruled out entirely, the satellite observations clearly demonstrate the large scale activation of dust over the southern Ukraine (Sect. 3.3). The total area of the Ukraine is 603, 700 km^2, 70% of which are used as farm lands. The southern Ukraine has been characterised as a *forest-steppe* zone, in its less droughty part, or as a *steppe* zone in its more droughty part. The precipitation is modest (350–400 mm p.a.) with average temperatures of 20°C in July. In both zones, human impact has almost completely removed the former native forests and steppe lands, and created large-scale agricultural units. The soil of the area is characterised by wide *loess* plains that have formed in the ice age under periglacial conditions. From loess, the very fertile black earth (Chernozem) has formed, which belongs to the most fertile soil types worldwide. Due to the intensive agricultural development, the soil has become prone to wind erosion and in fact, wind has been found to have eroded Ukrainian soils over an area of 220 000 km^2 (Dolgilevich, 1997)

Dolgilevich (1997) also presented an analysis of the frequency and effects of dusts storms in the Ukraine. Meteorological statistics over the past 40 years indicated that dust storms erode soils in all natural zones of the Ukraine. The frequency of dust storms was found to be 3–5 per year in the steppe zone, with an average duration of 8–17 h. Dust storms in the Ukraine are typically associated with wind speeds of 75 km h^{-1} and more. Chernozemic soils have been found to be the most susceptible to wind erosion. During dust storms, these soils can lose 70 t of soil per ha and hour.

5.5 Deforestation and desertification trends

Wind erosion of soils in the area of the former USSR have been recognised in the scientific literature as early as the 1920s and in fact, a considerable body of scientific studies (exclusively in Russian language) have been dedicated to the reasons of wind erosion and their environmental and economic consequences (a survey is given in Dolgilevich, 1997; Larionov et al., 1997). A prime reason for wind erosion is that

since the 1930s and particularly in the 1950s, many natural areas in the USSR were turned into intense agriculture. Currently, wind erosion in Eurasia gravitates to the southern forestless zone, where strong winds prevail. The areas of the most severe wind erosion are located in the European part and include the North Caucasus, Lower Don and, explicitely, the eastern and southern parts of Ukraine (Larionov et al., 1997). A comparision of the climate of the past (ca. 100 years ago) with the climate of today shows that the territory of the Ukraine has become arid due to human activities. Consequently, wind erosion has become wide-spread even in areas formerly unaffected by wind erosion.

It is currently unclear, whether the desertification trends will continue. As early as the 1950s, counter-actions have been devised to diminish wind erosion. Until now about 10% of the arable land has been transformed into untilled land. Also, systems of shelterbelts (coherent rows of trees) were planted in all the natural zones of the Ukraine. There are presently more than 440 000 ha of shelterbelts on agricultural fields (Larionov et al., 1997) with the main objective to decrease the near-surface wind speeds and therefore prevent dust activation.

As a matter of fact, the privatisation process in Ukraine has not relieved the pressure of intense agricultural use on the ecosystem (USAID, 2001). It appears uncertain how climate change might change the properties of the soil (further desertification?) as well as wind circulations in the mid-term future. Therefore, there is a considerable degree of uncertainty about the expected frequency of dust activation in the future, thereby affecting the neighbouring areas or even relatively distant areas like Central Europe.

It is also believed, but little researched, that increased dust storm activity has an impact on human health. Wiggs et al. (2003) report on a study that link increased dust exposure and respiratory health in the Autonomous Republic of Karakalpakstan, Uzbekistan, a region which is likewise affected by desertification trends.

An episode of extremely high PM concentrations over Central Europe

W. Birmili et al.

Title Page

Abstract	Introduction
Conclusions	References
Tables	Figures

◄◄ ►►

◄ ►

Back Close

Full Screen / Esc

Printer-friendly Version

Interactive Discussion

EGU

6 Conclusions

A comprehensive body of physical and chemical in situ aerosol measurements, remote sensing measurements as well as PM_{10} observations across Central Europe was used to depict an unusual occurrence of coarse dust advection into Central Europe on 24 March 2007. Rather than through lofted aerosol layers, as frequently observed with Saharan dust, the coarse dust entered into Central Europe within a fully developed boundary layer. Satellite images, backtrajectory calculations as well as meteorological status reports on a dust storm on 23 March strongly suggest the southern Ukraine (district of Kherson, around the Kakhovka Reservoir) as the main source region for this dust cloud. Owing to the meteorological constellation with a low pressure system over the Balkans, and a high pressure system over Central Russia, wind gusts up to $90\,\mathrm{km\,h^{-1}}$ occurred within the source region, and led to the activation of dust and its subsequent rapid transport in relatively dry air into Central Europe. Although an impact of Saharan dust cannot be ruled out on 24 March based on our backtrajectory analysis, the consideration of satellite as well as ground-based remote sensing observations make a significant contribution of Saharan dust unlikely.

PM_{10} measurement data from 360 monitoring stations were used to illustrate the advancement of the dust cloud across Slovakia, Poland, the Czech Republic, and Germany at an average speed of $70\,\mathrm{km\,h^{-1}}$. The peak PM_{10} concentrations were about $1400\,\mu\mathrm{g\,m^{-3}}$ in Slovakia, $1200\,\mu\mathrm{g\,m^{-3}}$ in Poland, and still around $600\,\mu\mathrm{g\,m^{-3}}$ in Germany. Lidar observations over Leipzig revealed that the high aerosol mass concentrations were confined to a homogeneous boundary layer of 1800 m height. The wavelength dependence of light extinction measurement using both lidar and sun photometer suggested the dominance of coarse particles on optical thickness during the main event. Also, relatively high volume extinction coefficients of $300\text{--}400\,\mathrm{Mm^{-1}}$ and a particle optical depth of 0.65 was observed at 532 nm.

In-situ measurements with an aerodynamic particle sizer at Melpitz, Germany confirmed the presence of a dominating coarse particle mode with a mode diameter

>2 μm, whose maximum concentration coincided that of PM_{10} mass concentration. Multiple point measurements across a horizontal distance of 200 km within the State of Saxony demonstrated a relatively homogeneous distribution of the atmospheric particle number size distribution as well as bulk PM_{10} particle chemical composition. The chemical analysis of PM_{10} samples confirmed the overwhelming presence of non-volatile and insoluble matter in the coarse mode as well as high enrichments of the geogenic elements Fe and Ti. Several approaches came to the same conclusion that the mass fraction of geogenic dust in daily average PM_{10} on 24 March was about 80%.

A screening of the long-term time series of PM_{10} mass concentration and chemical composition at Melpitz showed that there has in fact been no other case like 24 March 2007 between 1993 and 2007, i.e. there has been no other case in 14 years where the fraction of insoluble coarse dust in PM_{10} was so dominant. It is evident that as a result of the dust cloud on 24 March 2007 the legal daily limit value of PM_{10} (EU First Air Quality Daughter Directive (1999/30/EC)) was exceeded over an area spanning several EU member states. A question, and also a concern is whether such events of dust activation might become more frequent in the future as a result of continuing anthropogenic desertification processes.

A look at previous research showed that the problem of dust storms has been identified in the Ukraine and other regions of southern Eurasia since the 1950s. The motivation of looking at dust storms was the dramatic increase of wind erosion, which went along with the reclamation of large areas of land for intense agricultural use, and irrigation measures. Unfortunately, most new arable lands in the former USSR were reclaimed in areas of high wind speeds, so that desertification trends could have an immediate impact on wind erosion and the activation of ground dust.

Dust emissions from regions such as southern Eurasia are indeed anticipated to change under changed climate conditions due to alterations in both natural vegetation growth, cultivation patterns, and even meteorological transport pathways. An assessment of the role of dust in future climates will require the understanding of the controlling factors of dust emission, including the role of changes in land use, such as the

continuing destruction of soil crusts and removal of vegetation in semi-arid regions. In any case, our observation highlights the need to improve the description of large-scale dust emission fluxes under a changing climate as well as direct anthropogenic intervention, and models simulating 3-dimensional transport of coarse dust.

Appendix A

Sources of PM$_{10}$ network data

The various originators of the PM$_{10}$ network data used in this study are listed in Table 1. The half-hourly or hourly time series are particularly referred to in in Sect. 2.3. Table 1 indicates the number of observation sites for which the PM$_{10}$ time series were evaluated numerically in order to produce Fig. 7.

Appendix B

Charge correction of TDMPS mobility distributions using APS data

Since no measurement technique can measure particle size distributions across the wide size range between 3 nm and 10 μm with high accuracy, a combination of measurement techniques is usually deployed, depending of the actual purpose of the measurements. In this paper, we have utilized a combination of an electromobility spectrometer (TDMPS) and an aerodynamic particle sizer (APS).

Our electromobility spectrometer is based on Hauke differential mobility analysers (DMAs) that are fed with high voltages up to 12.5 kV (Birmili et al., 1999). At the given sheath-to-aerosol flow rate 5.0/0.5 l min^{-1}, the electromobility spectrometer selects particles at electromobility diameters up to 800 nm. The aerodynamic particle sizer (APS; model 3321, TSI Inc., St Paul, USA) (Peters and Leith, 2003), in contrast, measures

particles above an aerodynamic diameter of 835 nm. The aerodynamic diameter and the electromobility diameters can be connected by the so-called *effective particle density*, a lump parameter that describes the combined effects of particle material density as well as shape on aerosol motion. Schmid et al. (2007) have recently provided a comprehensive survey of the effects related to the effective particle density.

Every electromobility spectrometer measures number mobility distributions that still include the counts of multiply charged particles. Solving an inversion algorithm is necessary in order to obtain true particle number size distributions (Hagen and Alofs, 1983). The exact multiple charge inversion algorithm used in this paper is described in Stratmann and Wiedensohler (1996). As long as particles larger than the upper size limit of the electromobility spectrometer (here: 800 nm) are not removed physically, a correct multiple charge correction of the mobility distributions requires either the knowledge of the size distribution of larger particles, or the assumption that the concentration of larger particles decreases so strongly with particle size that their contributions on smaller mobility sizes are negligible.

As large numbers of coarse particles were detected during the dust episode described in this paper, their effect on the sub-μm mobility distribution could a priori not be ignored. In fact, particles >800 nm with a high number concentration and carrying a multiple number of charges after passing the diffusion charger upstream the DMAs, are expected to appear in the mobility raw spectrum <800 nm. As the number concentrations of particles >800 nm were, however, available through APS measurements, the effect of these multiply charged particles could be removed from the mobility raw distribution. Without this correction, the contributions of particles >800 nm would erroneously be interpreted as concentrations of particles <800 nm.

In practice, we employed the APS particle number size distribution in dN/dlogD_p measured simultaneously with the TDMPS at the same aerosol inlet in Melpitz. First, an effective particle density needs to be assumed. Here we assume an effective particle density of 2.0 g cm^{-3}, which corresponds to the magnitude of soil dust density. Second, the number of particles $N(D_p)$ from any channel of the APS size distribution

needs to be calculated, whose mobility diameters are lower than 800 nm. Since the mobility is a function of the charge, we accounted for multiple charges up to n=15, which includes more than 99% of the total of the multiply charged particles. To calculate the bipolar charge distribution $F(D_p, n_e)$ the experimentally derived Gunn-distribution for the particle charging efficiency in air as a function of particle diameter and charge was used (Wiedensohler, 1988). The product $0.5 \cdot F(D_p, n_e) \cdot N(D_p)$ needs to be subtracted from the number of particles of the appropriate TDMPS mobility raw spectrum. (Note that the factor 0.5 originates from the asymptotic value of the DMA transfer function area for large particle sizes.) This procedure reduces the number of particles in the mobility raw spectrum, and also in the final particle size distribution after the inversion routine.

Figure 15 shows the inverted TDMPS particle size distributions as a function of mobility diameter with and without correction for particles >800 nm as well as the APS number size distribution converted to electromobility diameters using an effective density of ρ=2.0 g cm^{-3} (cf., e.g., Maring et al., 2003). Figure 15 shows number as well as volume size distributions assuming spherical particles. Both graphs show data during the time of peak concentration occurring between 11:15–12:15 CET.

Two main effects are evident: First, the correction procedure reduces the TDMPS size distributions at the upper end by relative values up to 40%, which justifies the necessity of the correction scheme. Second, the TDMPS and APS size distributions appear to match better in the overlap region of both instruments after applying the correction. This clearly shows the need for a combined TDMPS/APS evaluation scheme during combined measurements if considerable amounts of coarse aerosol particles are present.

It is useful to note that for periods without high concentrations of coarse dust, the effects of the correction procedure were minor, and typically had an effect below 0.5% on the TDMPS concentrations at the upper end. Under average conditions, TDMPS size distributions can be safely inverted without the correction procedure using APS data.

An episode of extremely high PM concentrations over Central Europe

W. Birmili et al.

References

Ackerman, S. A.: Remote sensing aerosols using satellite infrared observations, J. Geophys. Res, 102, 17 069–17 079, 1997. 12236

Allen, G., Sioutas, C., Koutrakis, P., Reiss, R., Lurmann, F. W., and Roberts, P. T.: Evaluation of the TEOM method for measurement of ambient particulate mass in urban areas, J. Air Waste Manage. Assoc., 47, 682–689, 1997. 12238

Alpert, P., Kishcha, P., Shtivelman, A., Krichak, S. O., and Joseph, J. H.: Vertical distribution of Saharan dust based on 2.5-year model predictions, Atmos. Res., 70, 109–130, 2004. 12234

Althausen, D., Engelmann, R., Foster, R., Rhone, P., and Baars, H.: Portable Raman lidar for determination of particle backscatter and extinction coefficients, in Reviewed and revised papers presented at the 22nd ILRC, edited by G. Pappalardo and A. Amodeo, vol. 1 of *ESA SP-561*, pp. 83–86, ESTEC, Noordwijk, The Netherlands, ESA Publications Division, 2004. 12237

Amiridis, V., Balis, D. S., Kazadzis, S., Bais, A., Giannakaki, E., Papayannis, A., and Zerefos, C.: Four-year aerosol observations with a Raman lidar at Thessaloniki, Greece, in the framework

An episode of extremely high PM concentrations over Central Europe

W. Birmili et al.

Title Page

Abstract	Introduction
Conclusions	References
Tables	Figures

◄ ►|

◄ ►

Back | Close

Full Screen / Esc

Printer-friendly Version

Interactive Discussion

of European Aerosol Research Lidar Network (EARLINET), J. Geophys. Res., 110, D21203, doi:10.1029/2005JD006190, 2005. 12233, 12245

Annesi-Maesano, I., Forastiere, F., Künzli, N., and Brunekreef, B.: Particulate matter, science and EU policy, Eur. Respir. J., 29, 428–431, 2007. 12235

5 Ansmann, A. and Müller, D.: Lidar and atmospheric aerosol particles, in LIDAR — Range-resolved optical remote sensing of the atmosphere, edited by C. Weitkamp, pp. 105–141, Springer, New York, 2005. 12237

Ansmann, A., Bösenberg, J., Chaikovsky, A., Comeron, A., Eckhardt, S., et al.: Long–range transport of Saharan dust to northern Europe: The 11–16 October 2001 outbreak observed

10 with EARLINET, J. Geophys. Res., 108, 4783, doi:10.1029/2003JD003757, 2003. 12233, 12245, 12251

Barkan, J., Alpert, P., Kutiel, H., and Kishcha, P.: Synoptics of dust transportation days from Africa toward Italy and central Europe, J. Geophys. Res., 110, D07208, doi:10.1029/2004JD005222, 2005. 12233, 12245

15 Belnap, J. and Gillette, D. A.: Disturbance of biological soil crusts: Impacts on potential wind erodibility of sandy desert soils in Southeastern Utah, Land Degrad. Devel., 8, 355–362, 1997. 12235

Birmili, W., Stratmann, F., and Wiedensohler, A.: Design of a DMA-Based Size Spectrometer for a Large Particle Size Range and Stable Operation, J. Aerosol Sci., 30, 549–553, 1999.

20 12239, 12262

Birmili, W., Wiedensohler, A., Heintzenberg, J., and Lehmann, K.: Atmospheric particle number size distributions in Central Europe: Statistical relations to air masses and meteorology, J. Geophys. Res., D23, 32 005–32 018, 2001. 12238

Birmili, W., Allen, A., Bary, F., and Harrison, R. M.: Trace metal concentrations and water

25 solubility in size-fractionated atmospheric particles and influence of road traffic, Env. Sci. Technol., 40, es0486925, 2006. 12255

Brindley, H. E. and Russell, J. E.: Improving GERB scene identification using SEVIRI: Infrared dust detection strategy, Remote Sens. Environ., 104, 426–446, 2006. 12236

Brockmann, J. E.: Sampling and transport of aerosols, in Aerosol Measurement: Principles,

30 Techniques and Applications, edited by P. A. Baron and K. Willeke, pp. 143, Wiley, New York, 2001. 12239

Brüggemann, E. and Rolle, W.: Changes of some components of precipitation in East Germany after the unification, Water Air Soil Poll., 107, 1–23, 1998. 12241

An episode of extremely high PM concentrations over Central Europe

W. Birmili et al.

Title Page

Abstract	Introduction
Conclusions	References
Tables	Figures

◄ | ►|

◄ | ►

Back | Close

Full Screen / Esc

Printer-friendly Version

Interactive Discussion

Charron, A., Harrison, R. M., and Quincey, P.: What are the sources and conditions responsible for exceedences of the 24 h PM10 limit value (50 μg m^{-3}) at a heavily trafficked London site?, Atmos. Environ., 41, 1960–1975, 2007. 12235

Dolgilevich, M. J.: Extent and Severity of Wind Erosion in the Ukraine, in International Symposium on Wind Erosion, Kansas State University, Manhattan, KA, USA, June 3–5, 1997. 12258

Donk, S. J. V. and Skidmore, E. L.: Measurement and simulation of wind erosion, roughness degradation and residue decomposition on an agricultural field, Earth Surface Processes and Landforms, 28, 1243–1258, 2003. 12235

Engler, C., Rose, D., Wehner, B., Wiedensohler, A., Brüggemann, E., Gnauk, T., Spindler, G., Tuch, T., and Birmili, W.: Size distributions of non-volatile particle residuals (D$_p$<800 nm) at a rural site in Germany and relation to air mass origin, Atmos. Chem. Phys. Discuss., 6, 10 403–10 424, 2006. 12238

Escudero, M., Querol, X., Ávila, A., and Cuevas, E.: Origin of the exceedances of the European daily PM limit value in regional background areas of Spain, Atmos. Environ., 41, 730–744, 2007. 12235

Fernandez-Espinosa, A. J., Rodriguez, M. T., de la Rosa, F. J. B., and Sanchez, J. C. J.: A chemical speciation of trace metals for fine urban particles, Atmos. Environ., 36, 773–780, 2002. 12253

Gillette, D. A.: A wind tunnel simulation of the erosion of soil: effect of soil texture, sandblasting, wind speed and soil consolidation on dust production, Atmos. Env., 12, 1735–1743, 1978. 12234

Gillette, D. A. and Chen, W. A.: Particle production and aeolian transport from a "supply-limited" source area in the Chihuahuan desert, New Mexico, United States, J. Geophys. Res., 106, 5267–5278, 2001. 12235

Goudie, A. S. and Middleton, N. J.: Saharan dust storms: nature and consequences, Earth Sci. Rev., 56, 179–204, 2001. 12234

Grover, B. D., Eatough, N. L., Eatough, D. J., Chow, J. C., Watson, J. G., et al.: Measurement of both nonvolatile and semi-volatile fractions of fine particulate matter in Fresno, CA, Aerosol Sci. Technol., 40, 811–826, 2006. 12240

Hagen, D. E. and Alofs, D. J.: Linear inversion method to obtain aerosol size distributions from measurements with a differential mobility analyzer, Aerosol Sci. Technol., 2, 465–475, 1983. 12263

An episode of extremely high PM concentrations over Central Europe

W. Birmili et al.

Title Page

Abstract	Introduction
Conclusions	References
Tables	Figures

◄ | ►|

◄ | ►

Back | Close

Full Screen / Esc

Printer-friendly Version

Interactive Discussion

EGU

Hagen, L. J.: Evaluation of the wind erosion prediction system (WEPS) erosion submodel on cropland fields, Env. Modell. Softw., 19, 171–176, 2004. 12235

Harrison, S. P., Kohfeld, K. E., Roelandt, C., and Claquin, T.: The role of dust in climate changes today, at the last glacial maximum and in the future, Earth Sci. Rev., 54, 43–80, 2001. 12233

5 Haywood, J. M., Francis, P. N., Glew, M. D., and Taylor, J. P.: Optical properties and direct radiative effect of Saharan dust: A case study of two Saharan dust outbreaks using aircraft data, J. Geophys. Res., 106, 18 417–18 430, 2001. 12233

Hildemann, L. M., Russel, A. G., and Cass, G. R.: Ammonia and nitric acid concentrations in equilibrium with atmospheric aerosols: experiment vs. Theory, Atmos. Environ., 18, 1737–

10 1750, 1984. 12240, 12252

Hinds, W. C.: Aerosol Technology: Properties, Behaviour and Measurement of Airborne Particles, John Wiley, New York, 2 edn., 1999. 12239

Holben, B. N., Kaufman, Y. K., Eck, T. F., Slutsker, I., Tanre, D., Buis, J. P., Setzer, A., Vermote, E., and Reagan, J.: AERONET — A federated instrument network and data archive for

15 aerosol characterization, Remote Sens. Environ., 66, 1–16, 1998. 12238

Larionov, G. A., Skidmore, E. L., and Kiryukhina, Z. P.: Wind Erosion in Russia: Spreading and Quantitative Assessment, in International Symposium on Wind Erosion, Kansas State University, Manhattan, KA, USA, June 3–5, 1997. 12258, 12259

Lenschow, P., Abraham, H. J., Kutzner, K., Lutz, M., Preuss, J. D., and Reichenbacher, W.:

20 Some ideas about the sources of PM10, Atmos. Environ., 35, S23–S33, 2001. 12235

Loosmore, G. A. and Hunt, J. R.: Dust resuspension without saltation, J. Geophys. Res., 105, 20 663–20 671, 2000. 12234

Macias, E. S. and Husar, R. B.: Atmospheric particulate mass measurement with beta attenuation mass monitor, Environ. Sci. Technol., 10, 904–907, 1976. 12238

25 Mahowald, N. and Luo, C.: A less dusty future? Geophys. Res. Lett., 30, 2003GL017880, 2003. 12233

Maring, H., Savoie, D. L., Izaguirre, M. A., Custals, L., and Reid, J. S.: Mineral dust aerosol size distribution change during atmospheric transport, J. Geophys. Res., 108, 8592, doi:10.1029/2002JD002536, 2003. 12239, 12264

30 Marticorena, B. and Bergametti, G.: Modeling the atmospheric dust cycle: 1. design of a soil-derived dust emission scheme, J. Geophys. Res., 100, 16 415–16 430, 1995. 12234, 12235

Mattis, I., Ansmann, A., Müller, D., Wandinger, U., and Althausen, D.: Dual-wavelength Raman lidar observations of the extinction-to-backscatter ratio of Saharan dust, Geophys. Res. Lett.,

An episode of extremely high PM concentrations over Central Europe

W. Birmili et al.

Title Page

Abstract	Introduction
Conclusions	References
Tables	Figures

|◄ | ►|

◄ | ►

Back | Close

Full Screen / Esc

Printer-friendly Version

Interactive Discussion

EGU

29, doi:10.1029/2002GL014721, 2002. 12251

Mattis, I., Ansmann, A., Müller, D., Wandinger, U., and Althausen, D.: Multiyear aerosol observations with dual-wavelength Raman lidar in the framework of EARLINET, J. Geophys. Res., 109, D13203, doi:10.1029/2004JD004600, 2004. 12250

5 Merchant, C. J., Embury, O., Borgne, P. L., and Bellec, B.: Saharan dust in nighttime thermal imagery: Detection and reduction of related biases in retrieved sea surface temperature, Remote Sens. Environ., 104, 15–30, 2006. 12236

Müller, D., Mattis, I., Wandinger, U., Ansmann, A., Althausen, D., Dubovik, O., Eckhardt, S., and Stohl, A.: Saharan dust over a Central European EARLINET-AERONET site: Com-
10 bined observations with raman lidar and sun photometer, J. Geophys. Res., 108, 4345, doi:10.1029/2002JD002918, 2003. 12251

Müller, K., Spindler, G., Maenhaut, W., Hitzenberger, R., Wieprecht, W., Baltensperger, U., and ten Brink, H.: INTERCOMP2000, a campaign to assess the comparability of methods in use in Europe for measuring aerosol composition, Atmos. Env., 38, 6459–6466, 2004. 12238

15 Neusüss, C., Brüggemann, E., and Herrmann, H.: Determination of water-soluble organic ions of size-segregated aerosol particles by capillary zone electrophoresis, in Proceedings of the EUROTRAC Symposium 1998, edited by P. Borrell, vol. 1, pp. 639–643, WITPRESS, Southampton, UK, 1999. 12241

Neusüss, C., Wex, H., Birmili, W., Wiedensohler, A., Koziar, C., Busch, B., Brüggemann, E.,
20 Gnauk, T., Ebert, M., and Covert, D. S.: Characterization and parameterization of atmospheric particle number, mass, and chemical size distributions in central Europe during LACE 98 and MINT, J. Geophys. Res., 107, 8127, doi:10.1029/2001JD000514, 2002. 12238

Nilsson, E. D., Pirjola, L., and Kulmala, M.: The effect of atmospheric waves on aerosol nucleation and size distribution, J. Geophys. Res., 105, 19 917–19 926, 2000. 12249

25 Nilsson, E. D., Rannik, U., Kulmala, M., Buzorius, G., and O'Dowd, C. D.: Effects of continental boundary layer evolution, convection, turbulence, and entrainment on aerosol formation, Tellus, 53B, 441–461, 2001. 12249

Peters, T. M. and Leith, D.: Concentration measurement and counting efficiency of the aerodynamic particle sizer 3321, J. Aerosol Sci., 34, 627–634, 2003. 12239, 12262

30 Plewka, A., Gnauk, T., Brüggemann, E., Neusüß, C., and Herrmann, H.: Size-resolved aerosol characterisation for a polluted episode at the IfT research station Melpitz in Autumn 1997, J. Atmos. Chem., 48, 131–156, 2004. 12241

Prospero, J. M., Ginoux, P., Torres, O., Nicholson, S. E., and Gill, T. E.: Environmental char-

ACPD

7, 12231–12288, 2007

An episode of extremely high PM concentrations over Central Europe

W. Birmili et al.

Title Page

Abstract	Introduction
Conclusions	References
Tables	Figures

◄ | ►|

◄ | ►

Back | Close

Full Screen / Esc

Printer-friendly Version

Interactive Discussion

EGU

acterization of global sources of atmospheric soil dust identified with the Nimbus 7 Total Ozone Mapping Spectrometer (TOMS) absorbing aerosol product, Rev. Geophys., 40, 1002, doi:10.1029/2000RG000095, 2002. 12234

Putaud, J.-P., Raes, F., Dingenen, R. V., Brüggemann, E., Facchini, M.-C., et al.: A European aerosol phenomenology – 1: chemical characteristics of particulate matter at kerbside, urban, rural and background sites in Europe, Atmos. Environ., 38, 2579–2595, 2004. 12236

Pye, K.: Aeolian dust and dust deposition, Academic Press, London, 1987. 12234

Reid, E. A., Reid, J. S., Meier, M. M., Dunlap, M. R., Cliff, S. S., Broumas, A., Perry, K., and Maring, H.: Characterization of African dust transported to Puerto Rico by individual particle and size segregated bulk analysis, J. Geophys. Res., 108, 8591, doi:10.1029/2002JD002935, 2003. 12233

Reimer, E., Scherer, B., Klug, W., and Yamartino, R. J..: A meteorological database for next-generation dispersion models, and a Lagrangian particle model based on kinematic simulation theory, Int. J. Env. Poll., 5(4–6), 623–634, 1995.

Reimer, E. and Scherer, B..: An operational meteorological diagnostic system for regional air pollution analysis and long-term modelling, Air Poll. Modelling and its Applications IX., Plenum Press, New York, 1992. 12241

Satheesh, S. K. and Moorthy, K.: Radiative effects of natural aerosols: A review, Atmos. Environ., 39, 2089–2110, 2005. 12233

Schepanski, K., Tegen, I., Laurent, B., Heinold, B., and Macke, A.: A new Saharan Dust Source Activation Frequency Map derived form MSG-SEVIRI IR-channels, Geophys. Res. Lett., in press, 2007.

Schmetz, J., Pili, P., Themkes, S., Just, D., Kerkmann, J., Rota, S., and Ratier, A.: An introduction to Meteosat Second Generation (MSG), Bull. Am. Meteorol. Soc., 83, pp. 977, 2002. 12237

Schmid, O., Karg, E., Hagen, D. E., Whitefield, P. D., and Ferron, G. A.: On the effective density of non-spherical particles as derived from combined measurements of aerodynamic and mobility equivalent size, J. Aerosol Sci., 38, 431–443, 2007. 12263

Shao, Y.: Physics and Modelling of Wind Erosion, Kluwer Academic Publishers, Dordrecht, The Netherlands, 2000. 12234

Shao, Y., Raupach, M. R., and Findlater, P. A.: Effect of saltation bombardment on the entrainment of dust by wind, J. Geophys. Res., 98, 12 719–12 726, 1993. 12234

Sokolik, I. N.: The spectral radiative signature of wind-blown mineral dust: Implica-

tions for remote sensing in the thermal IR region, Geophys. Res. Lett., 29, 2154. doi:10.1029/2002GL015910, 2002. 12236

Sokolik, I. N., Winker, D. M., Bergametti, G., Gillette, D. A., Carmichael, G., Kaufman, Y. J., Gomes, L., Schütz, L., and Penner, J. E.: Introduction to special section: Outstanding problems in quantifying the radiative impacts of mineral dust, J. Geophys. Res., 106, 18 015–18 027, 2001. 12233

Solomon, S., Qin, D., Manning, M., Chen, Z., Marquis, M., Averyt, K. B., Tignor, M., and Miller, H. L., eds.: Climate Change 2007: The Physical Science Basis, IPCC, Cambridge Univ. Press, Cambridge, United Kingdom, contribution of Working Group I to the Fourth Assessment Report of the Intergovernmental Panel on Climate Change (IPCC), 2007. 12233, 12234

Spindler, G., Müller, K., Brüggemann, E., Gnauk, T., and Herrmann, H.: Long-term size-segregated characterization of PM10, PM2.5, and PM1 at the IfT research station Melpitz downwind of Leipzig (Germany) using high and low-volume filter samplers, Atmos. Environ., 38, 5333–5347, 2004. 12238

Stratmann, F. and Wiedensohler, A.: A New Data Inversion Algorithm for DMPS Measurements, J. Aerosol Sci., 27, Suppl. 1, S339–S340, 1996. 12263

Taylor, S. R. and McLennan, S. M.: The Continental Crust: Its Composition and Evolution, Blackwell Science, Oxford, UK, 1985. 12255

Tegen, I., Werner, M., Harrison, S. P., and Kohfeld, K. E.: Relative importance of climate and land use in determining present and future global soil dust emission, Geophys. Res. Lett., 31, L05105, doi:10.1029/2003GL019216, 2004. 12233

Textor, C., Schulz, M., Guibert, S., Kinne, S., Balkanski, Y., et al.: Analysis and quantification of the diversities of aerosol life cycles within AeroCom, Atmos. Chem. Phys., 6, 1777–1813, 2006,
http://www.atmos-chem-phys.net/6/1777/2006/. 12233

USAID: Biodiversity Assessment for Ukraine: Task Order under the Biodiversity and Sustainable Forestry IQC (BIOFOR), August 2001, USAID/Kiev, Kiev, Ukraine, 2001. 12259

Vautard, R., Bessagnet, B., Chin, M., and Menut, L.: On the contribution of natural Aeolian sources to particulate matter concentrations in Europe: Testing hypotheses with a modelling approach, Atmos. Environ., 39, 3291–3303, 2005. 12236

Wald, A. E., Kaufmann, Y. J., Tané, D., and Gao, B.-C.: Daytime and nighttime detection of mineral dust over desert using infrared spectral contrast, J. Geophys. Res., 103, 32 307–

Title Page

Abstract | Introduction

Conclusions | References

Tables | Figures

|◄ | ►|

◄ | ►

Back | Close

Full Screen / Esc

Printer-friendly Version

Interactive Discussion

EGU

32 313, 1998. 12236

Wiedensohler, A.: An approximation of the bipolar charge distribution for particles in the sub-micron range, J. Aerosol Sci., 19, 387–389, 1988. 12264

Wiggs, G. F. S., O'Hara, S. L., Wegerdt, J., Meer, J. V. D., Small, I., and Hubbard, R.: The dynamics and characteristics of Aeolian dust in dryland Central Asia: possible impacts on human exposure and respiratory health in the Aral Sea basin, Geograph. J., pp. 169, 2003. 12259

Woodward, S., Roberts, D. L., and Betts, R. A.: A simulation of the effect of climate change-induced desertification on mineral dust aerosol, Geophys. Res. Lett., 32, L18810, doi:10.1029/2005GL023482, 2005. 12233

Zender, C., Miller, R., and Tegen, I.: Quantifying mineral dust mass budgets: Systematic termi-nology, constraints, and current estimates, EOS, 85, 509–512, 2004. 12233

An episode of extremely high PM concentrations over Central Europe

W. Birmili et al.

Title Page

Abstract | Introduction
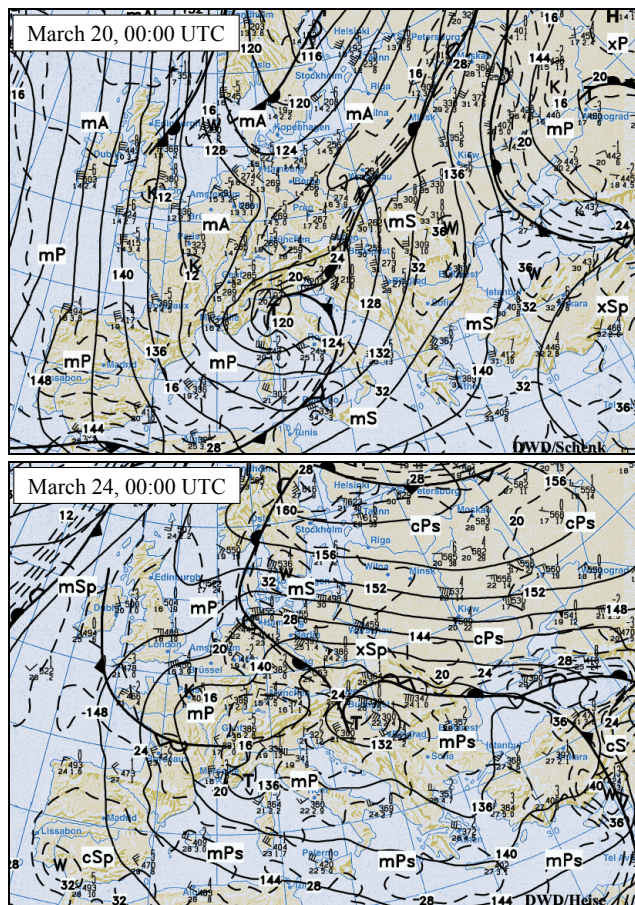
Conclusions | References

Tables | Figures

◄ | ►

◄ | ►

Back | Close

Full Screen / Esc

Printer-friendly Version

Interactive Discussion

EGU

Table 1. Originators of the PM$_{10}$ network data used in this study. Indicated is the total number of observation sites for PM$_{10}$ as well as the number of sites for which the PM$_{10}$ time series were evaluated numerically in order to produce Fig. 7.

Data originator	total	evaluated
Ceský hydrometeorologický ústav (Czech Hydrometeorological Institute, Prague, Czech Republic)	74	73
Slovenský hydrometeorologický ústav (Slovakian Hydrometeorological Institute, Bratislava, Slovakia)	25	23
Wojewódzki Inspektorat Ochrony Środowiska we Wrocławiu (Environmental inspectorate for Lower Silesia in Wrocław, Poland)	49	43
Österreichisches Umweltbundesamt (Austrian federal environment agency, Vienna, Austria)	101	4
Umweltbundesamt (German federal environment agency, Dessau, Germany	4	4
Sächsisches Landesamt für Umwelt und Geologie (Saxonian Office for the Environment and Geology, Dresden)	24	24
Thüringer Landesanstalt für Umwelt und Geologie (Office for the environment and geology in Thuringia, Erfurt, Germany)	21	21
Landesamt für Umweltschutz Sachsen-Anhalt (Office for environmental protection in Saxony-Anhalt, Magdeburg, Germany)	20	20
Ministerium für ländliche Entwicklung, Umwelt und Verbraucherschutz Brandenburg (Department for rural affairs, the environment, and customer protection in Brandenburg, Potsdam, Germany)	22	22
Lufthygienisches Überwachungssystem Niedersachsen (Air quality monitoring system in Lower Saxony, Hanover, Germany)	30	29
Bayerisches Landesamt für Umwelt (Bavarian office for the environment, Augsburg, Germany)	51	25
Hessisches Landesamt für Umwelt und Geologie (Office for the Environment and Geology in Hassia, Wiesbaden, Germany)	20	17
Bremer Senator für Bau, Umwelt und Verkehr (Senator for construction, the environment, and traffic in Bremen, Germany)	8	8
Landesamt für Umwelt, Naturschutz und Geologie Mecklenburg-Vorpommern (Office for the environment, the protection of nature and geology Mecklenburg-Vorpommern, Schwerin, Germany)	10	10
Ministerium für Landwirtschaft, Umwelt und ländliche Räume des Landes Schleswig-Holstein (Ministry for agriculture, the environment and rural areas Schleswig-Holstein, Kiel, Germany)	4	4

An episode of extremely high PM concentrations over Central Europe

W. Birmili et al.

Title Page

Abstract | Introduction

Conclusions | References

Tables | Figures

◄ | ►

◄ | ►

Back | Close

Full Screen / Esc

Printer-friendly Version

Interactive Discussion

EGU

Fig. 1. Synoptic chart of 850 hPa geopotential, wind observations and air masses over Europe, **(a)** 20 March, 00:00 UTC, **(b)** 20 March, 00:00 UTC.
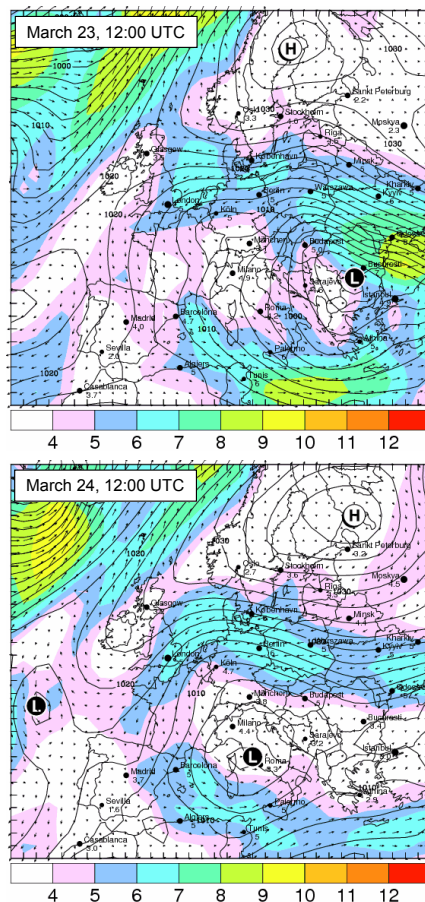
Fig. 2. Charts of sealevel pressure (hPa) and horizontal surface wind speeds in Beaufort (colour code) on 23 and 24 March 2007, 12:00 UTC respectively. The charts were produced using the MM5 model and selected from the EURAD products offered by the University of Cologne, Germany (http://www.eurad.uni-koeln.de, as of 11 June 2007).

An episode of extremely high PM concentrations over Central Europe

W. Birmili et al.

Title Page

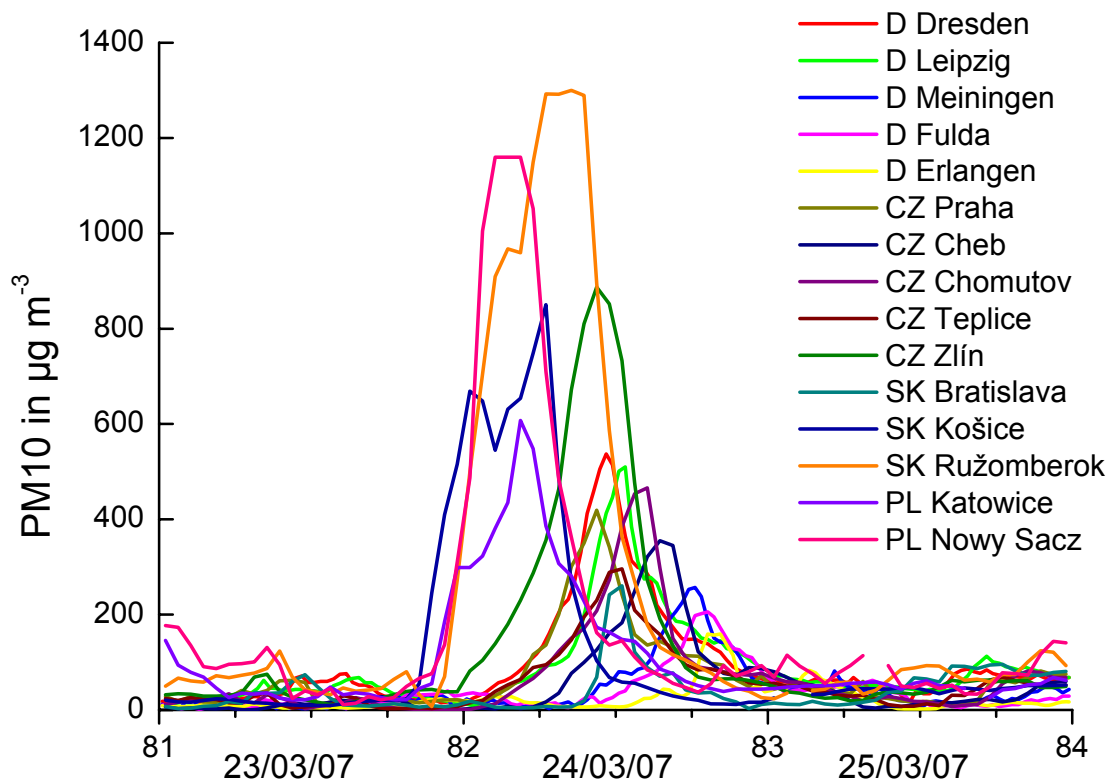| Abstract | Introduction |
| Conclusions | References |
| Tables | Figures |

◄◄ | ►►

◄ | ►

Back | Close

Full Screen / Esc

Printer-friendly Version

Interactive Discussion

EGU
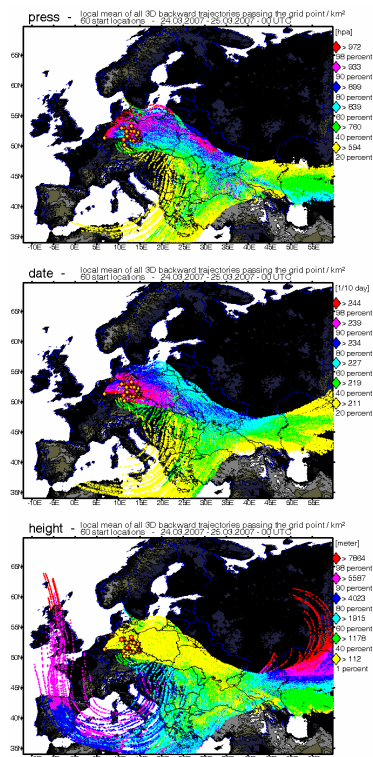
Fig. 3. Superposition of back trajectories originating on 24 March 2007 at 20 receptor sites in Germany. Colour coding indicates pressure (top graph), date (centre graph), and height above the ground (bottom graph) sampled for cells of $1\,km^2$. For each receptor site three types of trajectories were calculated in order to account for a spectrum of gravitational settling velocities of coarse particles (0, 0.5, and $1.0\,mm\,s^{-1}$). The graphs demonstrate the air mass origin in the southern Ukraine, where an easterly and a southerly air flow merge. From passing across the southern Ukraine, transport takes place within the boundary layer. Particles from the southerly flow across the Mediterranean can only enter into the boundary layer if sedimentation is taken into account.

Copyright EUMETSAT
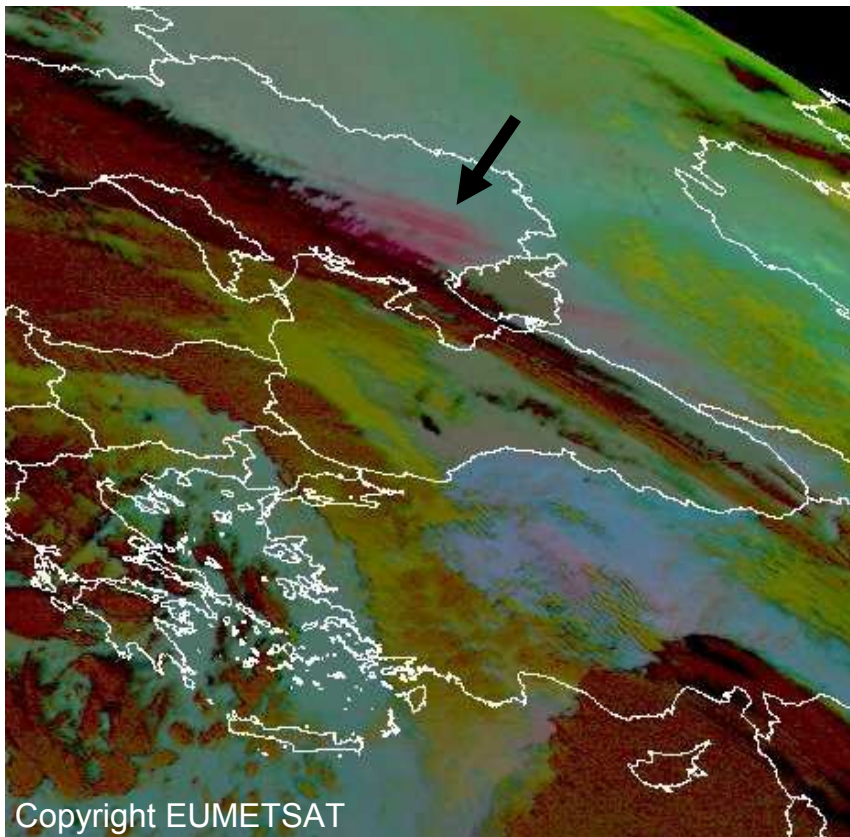
Fig. 4. Dust source activation on 23 March 11:00 UTC over the southern Ukraine (arrow). The image shows MSG dust index images, based on BTD using the 8.7 μm, 10.8 μm and 12.0 μm wavelength bands of the SEVIRI instrument (cf. Sect. 2.1). Magenta colour indicates dust, green colour low-level clouds, brown colour thick mid-level clouds and dark red colour thick high-level clouds. Copyright (2007) EUMETSAT, Darmstadt, Germany.
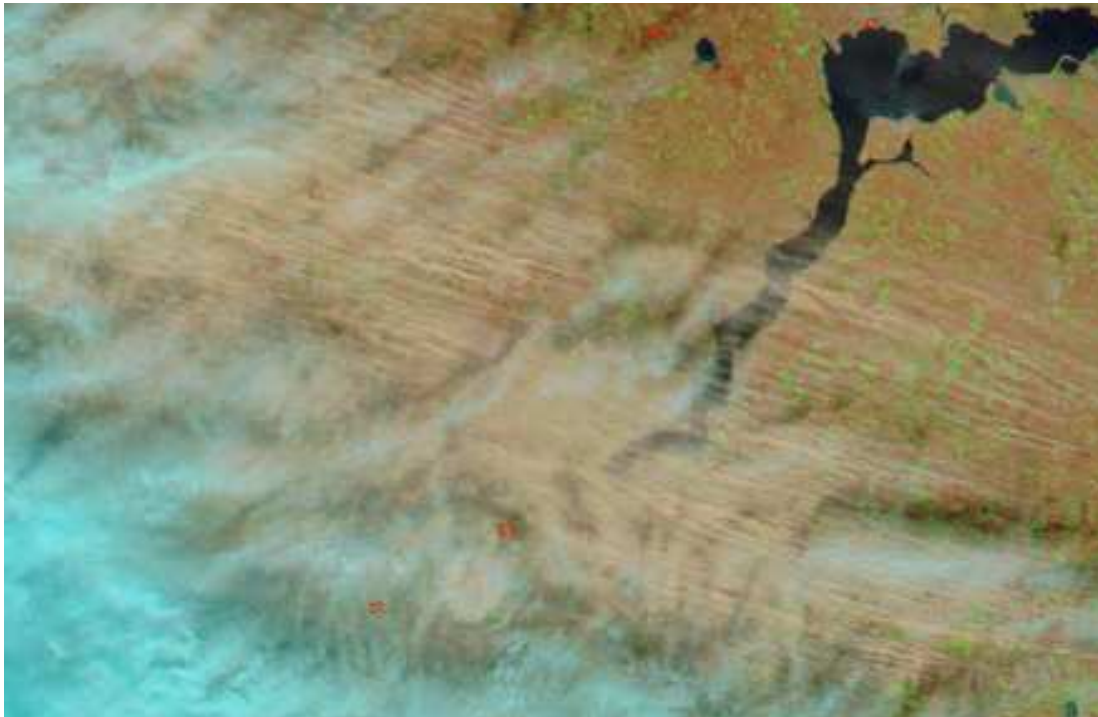
Fig. 5. MODIS-Aqua composite image of Southern Ukraine on 23 March 2007, 10:50 UTC reveals the large scale emission of agricultural dust. The reservoir lake of Kakhovskaya on the Dnieper River can be seen in dark blue, ice clouds in light blue. Red boxes indicates thermal anomalies, caused in most cases by fire or even flares from a gas well. The dimensions of the area shown is 210×146 km.

Title Page

Abstract   Introduction

Conclusions   References

Tables   Figures

◀   ▶▮

◀   ▶

Back   Close

Full Screen / Esc

Printer-friendly Version

Interactive Discussion

Fig. 6. Time series of PM$_{10}$ mass concentrations at a number of selected air quality monitoring stations in Slovakia, the Czech Republic, Poland, and Germany. The data show the singular and short-lived nature of the dust cloud as measured across the networks of stations.
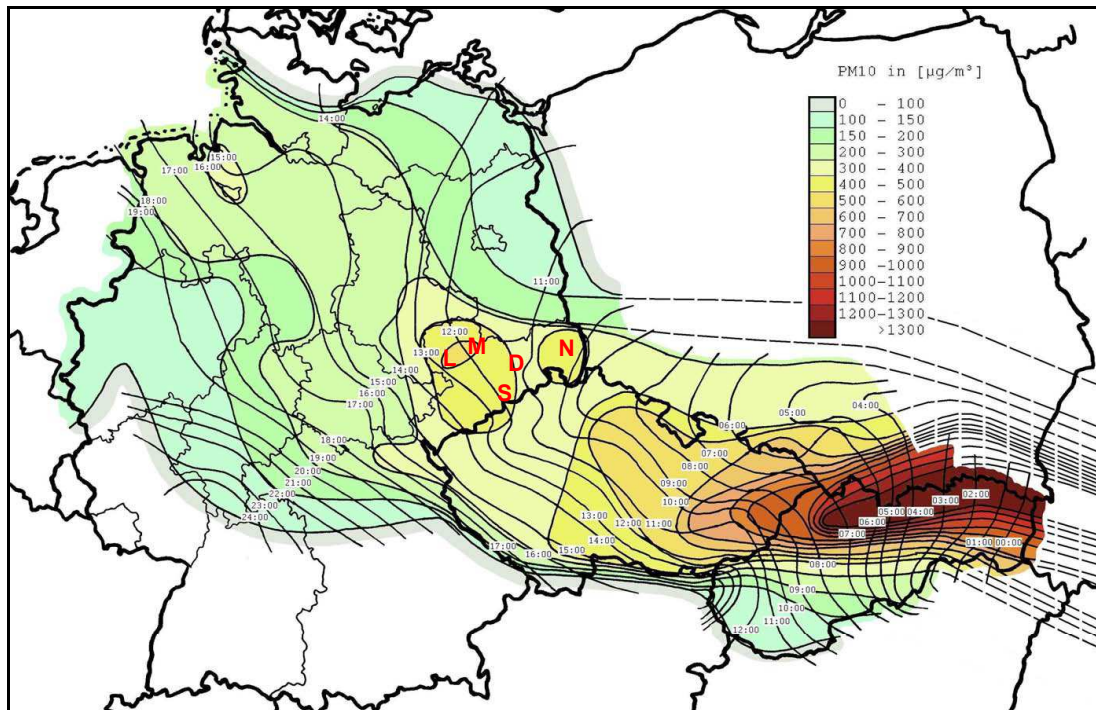
Fig. 7. Spatio-temporal evolution of the dust cloud in Central Europe on 24 March 2007. The map is based on the evaluation of time series of PM_{10} mass concentration at over 360 governmental monitoring stations in Slovakia, the Czech Republic, Austria, Poland, and Germany. The labelled lines represent the frontal lines of the dust cloud, i.e. where the peak values of PM_{10} occurred simultaneously. The peak PM_{10} concentrations are coded in colour. The edge of the dust cloud is marked in grey if well supported by the observational data. Additional markers indicate the measurement locations Leipzig (L), Melpitz (M), Niesky (N), Schwartenberg (S) and Dresden (D). Dashed isolines of concentration represent extrapolations along backtrajectories over areas of missing data.

Title Page

Abstract | Introduction

Conclusions | References

Tables | Figures

◄ | ►◄

◄ | ►

Back | Close

Full Screen / Esc

Printer-friendly Version

Interactive Discussion

EGU
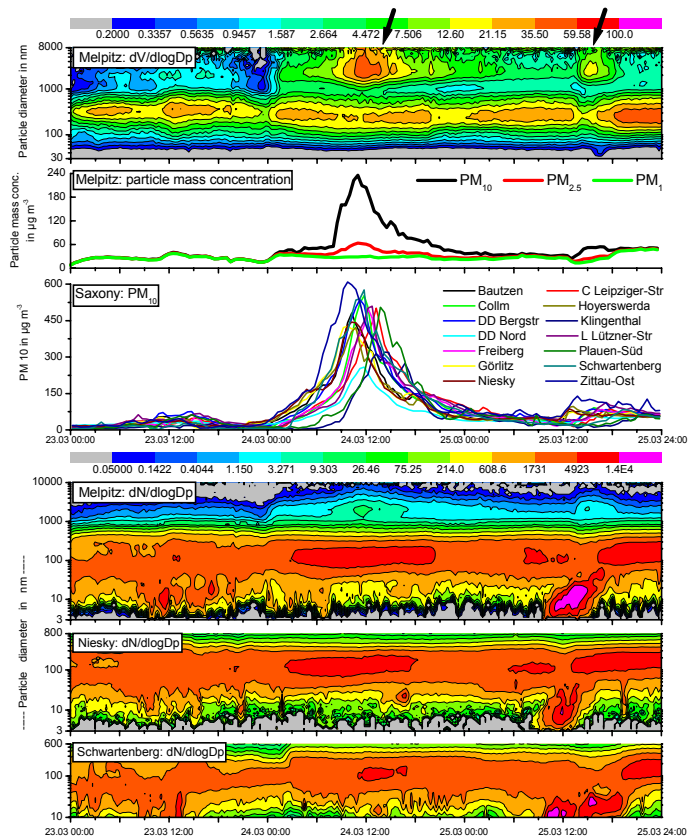
Fig. 8. In situ aerosol observations in Saxony, Germany, between 23 and 25 March 2007. Two events of high coarse particle concentrations are marked by arrows. Top graph: Particle volume size distribution measured by TDMPS and APS at Melpitz. Lower top graph: Particle mass concentration measured by the Grimm EDM. Third graph: PM$_{10}$ mass concentration at 14 monitoring stations measured by TEOM. Bottom graphs: Particle number size distribution measured by TDMPS and APS at three rural background stations, Melpitz, Niesky and Schwartenberg. Times are given in CET.

EGU
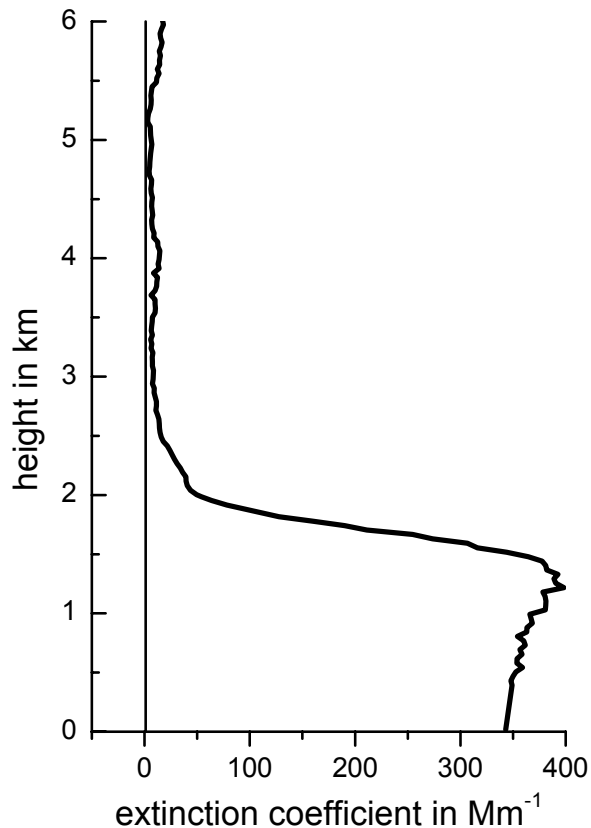
Fig. 9. Vertical profile of the volume extinction coefficient of the aerosol particles retrieved from Lidar observations at 532 nm wavelength at Leipzig, on 24 March 2007, 12:33–13:44 UTC. The height of the dust layer is about 1800 m. The free troposphere was almost deplete of aerosol and clouds during the observation period. Below 500 m height, the extinction coefficient is estimated by extrapolating the profile shape down to the ground. The particle optical depth is 0.65 at 532 nm.

Title Page

Abstract | Introduction

Conclusions | References

Tables | Figures

◄ | ►

◄ | ►

Back | Close

Full Screen / Esc

Printer-friendly Version

Interactive Discussion

EGU
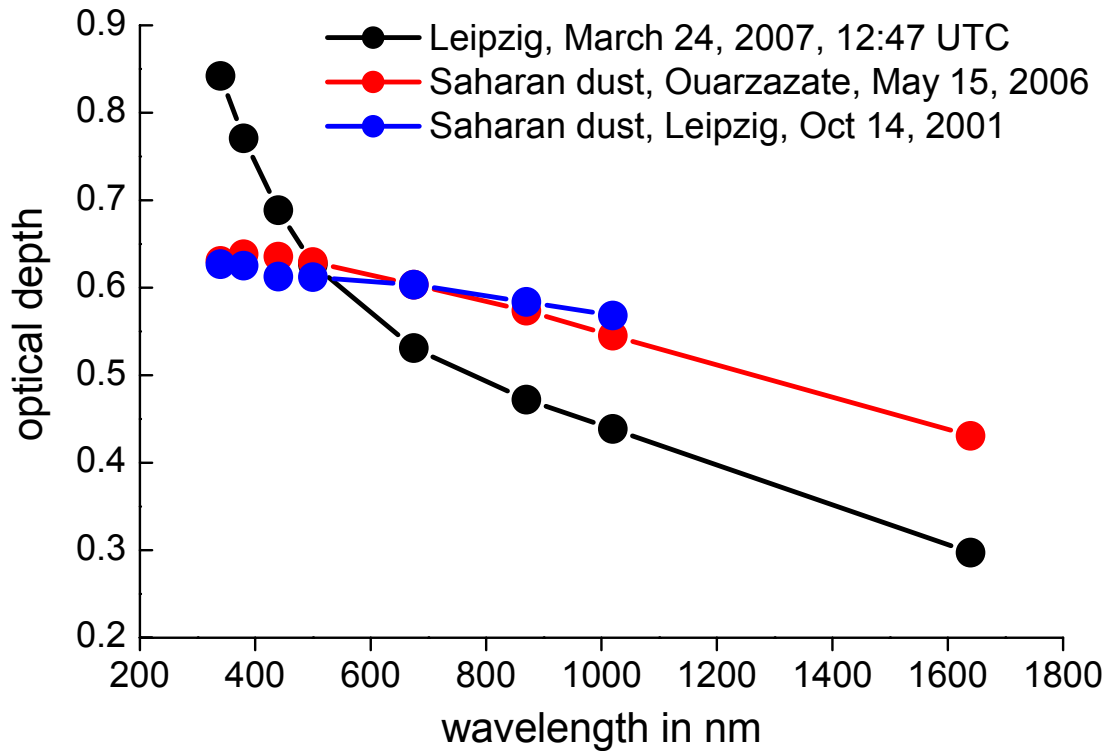
Fig. 10. Particle optical depth as a function of wavelength as retrieved from AERONET's sun photometer in Leipzig. The data from 24 March 2007 are complemented by two cases featuring Saharan dust aerosol: Ouarzazate, Southern Morocco, on 15 May 2006, 06:41–08:31 UTC, and Leipzig, 14 October 2001, 10:42–11:42 UTC. All the measurements shown were performed using the same sun photometer.

Title Page

Abstract | Introduction

Conclusions | References

Tables | Figures

◄ | ►

◄ | ►

Back | Close

Full Screen / Esc

Printer-friendly Version

Interactive Discussion

EGU
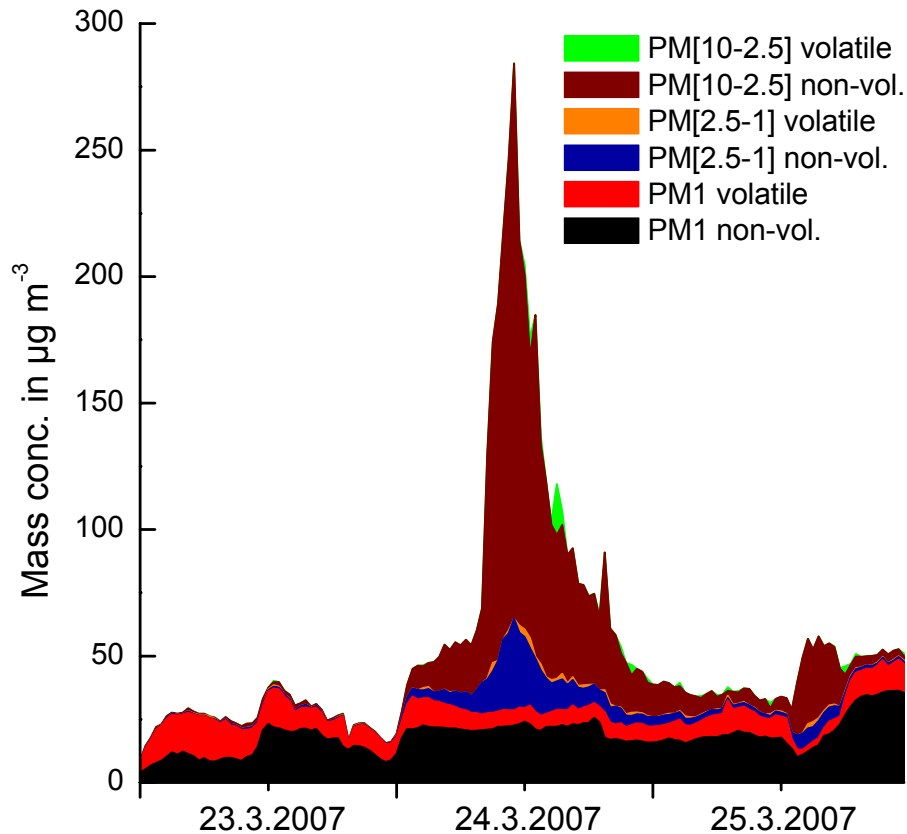
Fig. 11. Concentrations of the volatile and non-volatile mass fractions between 23 and 25 March 2007 in Melpitz, based on measurements using the Grimm Environmental Dust Monitor (EDM).

March 23 **March 24** **March 25**

PM$_{10}$ 23.73 (100%)   83.84 (100%)   39.69 (100%) µg/m³

PM$_{2.5}$ 20.20 (85%)   47.52 (57%)   30.71 (77%) µg/m³

PM$_{10}$-PM$_{2.5}$ 3.53 (15%)   36.32 (43%)   8.97 (23%) µg/m³

☐ Cl ☐ NO3 ☐ SO4 ☐ Na ☐ NH4 ☐ K ☐ Mg ☐ Ca ☐ OC ■ EC ■ Rest
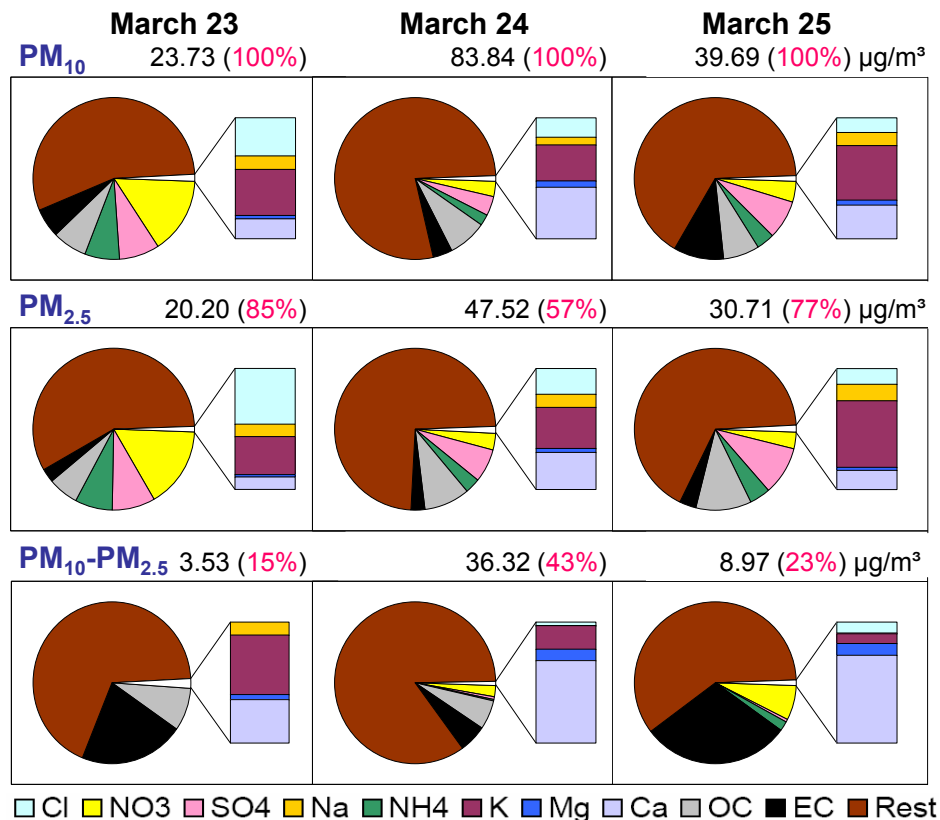
Fig. 12. Main components of bulk PM on 23 March (clean air mass), 24 March (dust event), and 25 March (continental air mass) at Melpitz. The circular charts indicate relative mass fractions, and total mass concentrations are added for clarity.

Title Page

Abstract   Introduction

Conclusions   References

Tables   Figures

◀◀   ▶▶

◀   ▶

Back   Close

Full Screen / Esc

Printer-friendly Version

Interactive Discussion

EGU
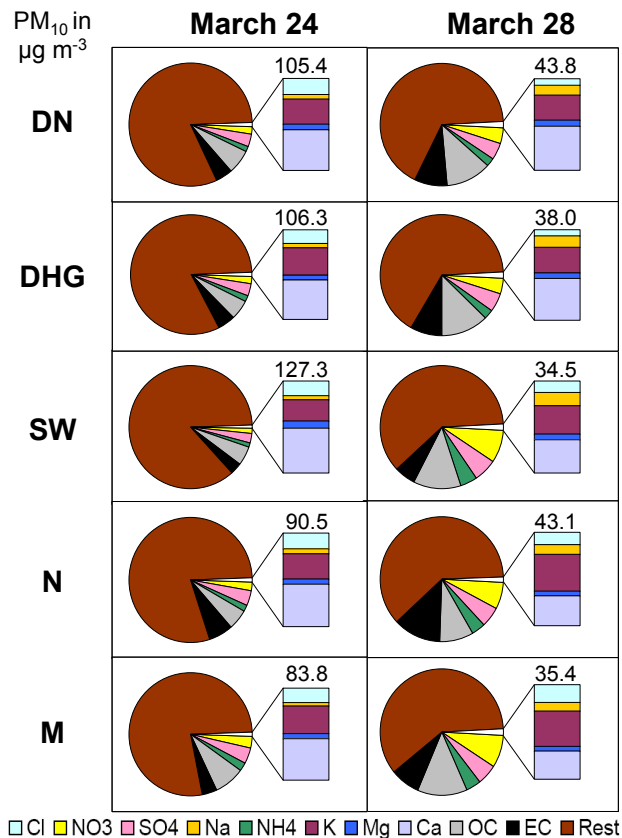
Fig. 13. Spatial variation of chemical composition: Main components of bulk PM_{10} on 24 March, the day of the dust event, and 28 March, the comparison day featuring continental background aerosol. The data is shown for the 5 sampling sites Dresden-Nord (DN), Dresden-Herzogingarten (DHG), Schwartenberg (SW), Niesky (N) and Melpitz (M) in Saxony, Germany (cf. Fig. 7).

Title Page

Abstract | Introduction
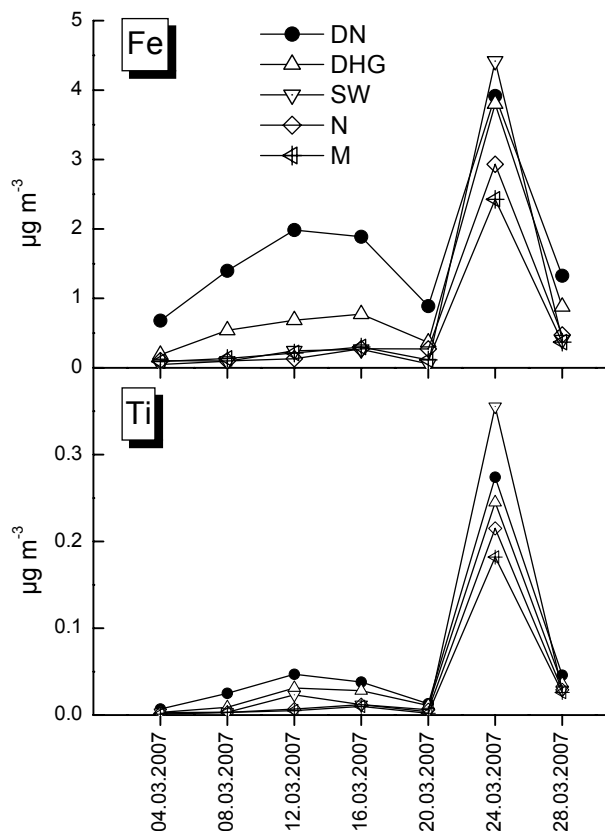
Conclusions | References

Tables | Figures

◄ | ►

◄ | ►

Back | Close

Full Screen / Esc

Printer-friendly Version

Interactive Discussion

EGU

**Fig. 14.** Daily average mass concentrations of iron (Fe) and Titanium (Ti) in PM_{10} at the 5 sampling sites Dresden-Nord (DN), Dresden-Herzogingarten (DHG), Schwartenberg (SW), Niesky (N) and Melpitz (M) in Saxony, Germany between 3 and 28 March 2007. 24 March corresponds to the day of the dust event over central Europe.

Title Page

Abstract | Introduction

Conclusions | References

Tables | Figures

◄ | ►

◄ | ►

Back | Close

Full Screen / Esc

Printer-friendly Version

Interactive Discussion

EGU
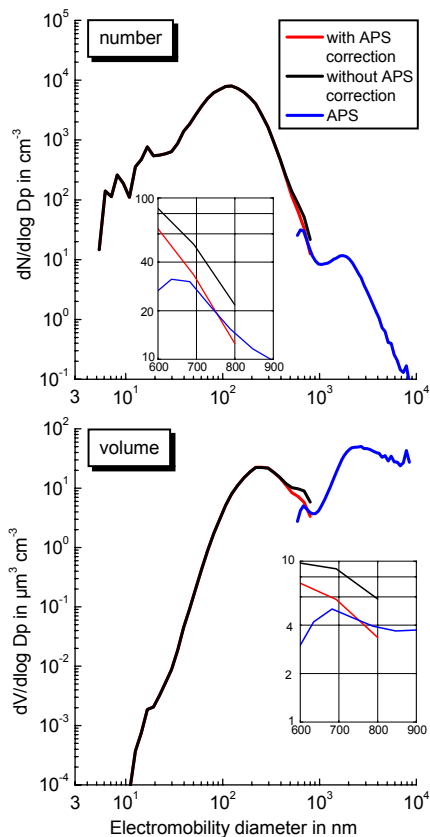
Fig. 15. Inverted TDMPS particle distributions with and without correction for particles >800 nm, and the APS number size distribution under the assumption of an effective particle density ρ=2.0 g cm^{-3}. The overlap region of both instruments between 600 and 800 nm is highlighted for clarity. The upper graph displays number size distributions, the lower graph volume size distributions assuming spherical partcles.

Title Page

Abstract | Introduction

Conclusions | References

Tables | Figures

|◄ | ►|

◄ | ►

Back | Close

Full Screen / Esc

Printer-friendly Version

Interactive Discussion

EGU